

# Contrasting thinning patterns between lake- and land-terminating glaciers in the Bhutan Himalaya

Shun Tsutaki<sup>1,a</sup>, Koji Fujita<sup>1</sup>, Takayuki Nuimura<sup>1,b</sup>, Akiko Sakai<sup>1</sup>, Shin Sugiyama<sup>2</sup>, Jiro Komori<sup>1,3,c</sup>, and Phuntsho Tshering<sup>1,3,d</sup>

5 <sup>1</sup>Graduate School of Environmental Studies, Nagoya University, Nagoya, Japan

<sup>2</sup>Institute of Low Temperature Science, Hokkaido University, Sapporo, Japan

<sup>3</sup>Department of Geology and Mines, Ministry of Economic Affairs, Thimphu, Bhutan

<sup>a</sup>now at: Atmosphere and Ocean Research Institute, The University of Tokyo, Kashiwa, Japan

<sup>b</sup>now at: Chiba Institute of Science, Choshi, Japan

10 <sup>c</sup>now at: Department of Modern Life, Teikyo Heisei University, Tokyo, Japan

<sup>d</sup>now at: Cryosphere Services Division, National Center for Hydrology and Meteorology, Thimphu, Bhutan

*Correspondence to:* Shun Tsutaki (tsutshun@frontier.hokudai.ac.jp)

**Abstract.** Despite the importance of glacial lake development in ice dynamics and glacier thinning, in situ and satellite-based measurements from lake-terminating glaciers are sparse in the Bhutan Himalaya, where a number of supraglacial lakes exist.

15 We acquired in situ and satellite-based observations across lake- and land-terminating debris-covered glaciers in the Lunana region, Bhutan Himalaya. A repeat differential global positioning system survey reveals that thinning of the debris-covered ablation area of the lake-terminating Lugge Glacier ( $-4.67 \pm 0.02 \text{ m a}^{-1}$ ) is more than three times greater than that of the land-terminating Thorthormi Glacier ( $-1.40 \pm 0.01 \text{ m a}^{-1}$ ) for the 2004–2011 period. The surface flow velocities decrease down-glacier along Thorthormi Glacier, whereas they increase from the upper part of the ablation area to the terminus of Lugge  
20 Glacier. Numerical experiments using a two-dimensional ice flow model demonstrate that the rapid thinning of Lugge Glacier is driven primarily by a negative surface mass balance and that the dynamically induced change in ice thickness is small. However, the thinning of Thorthormi Glacier is suppressed by a longitudinally compressive flow regime. The magnitude of dynamic ice thickening compensates the glacier thinning, suggesting that over half of the negative surface mass balance is counterbalanced by the ice dynamics of Thorthormi Glacier. Multiple ponds on Thorthormi Glacier have been expanding since  
25 2000 and merged into a single proglacial lake, with the glacier terminus detaching from its terminal moraine in 2011. Numerical experiments suggest that the speed up and thinning of Thorthormi Glacier will accelerate with continued proglacial lake development.

## 1 Introduction

The spatially heterogeneous shrinkage of Himalayan glaciers has been revealed by in situ measurements (Yao et al., 2012;  
30 Azam et al., 2018), satellite-based observations (Scherler et al., 2011a; Bolch et al., 2012; Käab et al., 2012; Brun et al., 2017), mass balance and climate models (Fujita and Nuimura, 2011; Mölg et al., 2014), and a compilation of multiple methods

(Cogley, 2016). Glaciers in Bhutan in the southeastern Himalayas have experienced significant shrinkage and thinning over the past four decades. For example, the Bhutanese glaciers shrank by  $13.3 \pm 0.1$  % between 1990 and 2010, based on repeated decadal glacier inventories (Bajracharya et al., 2014). Multitemporal digital elevation models (DEMs) revealed that the glacier-wide mass balance of Bhutanese glaciers was  $-0.17 \pm 0.05$  m w.e.  $a^{-1}$  during 1974–2006 (Maurer et al., 2016) and  $-0.22 \pm 0.12$  m w.e.  $a^{-1}$  during 1999–2010 (Gardelle et al., 2013). Bhutanese glaciers are inferred to be particularly sensitive to changes in air temperature and precipitation because they are affected by monsoon influenced humid climate conditions (Fujita, 2008; Sakai and Fujita, 2017). Tshering and Fujita (2016) reported a mass balance record of Gangju La Glacier in the central Bhutan Himalaya between 2003 and 2014, based on in situ measurements, where the glacier experienced much greater mass loss than neighbouring glaciers in the eastern Himalaya and southeastern Tibet. It is crucial to investigate the mechanisms driving the mass loss of Bhutanese glaciers to provide more accurate analyses of regional water availability (Immerzeel et al., 2010) and improve projections of global sea level rise and glacier evolution (Huss and Hock, 2018).

In recent decades, glacial lakes have formed and expanded at the termini of retreating glaciers in the Himalayas (Ageta et al., 2000; Komori, 2008; Fujita et al., 2009; Hewitt and Liu, 2010; Sakai and Fujita, 2010; Gardelle et al., 2011; Nie et al., 2017). Such proglacial lakes are dammed by terminal and lateral moraines, or stagnant ice masses at the glacial front (Sakai, 2012; Carrivick and Tweed, 2013). The formation and expansion of proglacial lakes accelerates glacier retreat through flotation of the terminus, increased calving, and ice flow (e.g., Funk and Röthlisberger, 1989; Warren and Kirkbride, 2003; Tsutaki et al., 2013). The ice thinning rates of lake-terminating glaciers are generally greater than those of neighbouring land-terminating glaciers in the Nepal and Bhutan Himalayas (Nuimura et al., 2012; Gardelle et al., 2013; Maurer et al., 2016; King et al., 2017). Increases in ice discharge and surface flow velocity at the glacier terminus cause rapid thinning due to longitudinal stretching, known as dynamic thinning. For example, dynamic thinning accounted for 17 % of the total ice thinning at lake-terminating Yakutat Glacier, Alaska, during 2007–2010 (Trüssel et al., 2013). Therefore, it is important to quantify the contributions of dynamic thinning and surface mass balance (SMB) to evaluate ongoing mass loss and predict the future evolution of lake-terminating glaciers in Bhutan.

To investigate the contribution of dynamically induced changes in ice thickness to glacier thinning, it is beneficial to compute the ice flow velocity field of a lake-terminating glacier using an ice flow model. Two-dimensional ice flow models have been utilised to investigate the dynamic thinning of marine-terminating outlet glaciers (Benn et al., 2007a; Vieli and Nick, 2011), which require the ice flow velocity field and glacier thickness. In Bhutan, ice flow velocity measurements have been carried out via remote sensing techniques with optical satellite images (Kääb, 2005; Bolch et al., 2012; Dehecq et al., 2015) and in situ global positioning system (GPS) surveys (Naito et al., 2012), but no ice thickness data are available. Another approach to investigate the relative importance of ice dynamics in glacier thinning is to compare lake- and land-terminating glaciers in the same region. This method has been applied to neighbouring lake- and land-terminating glaciers in Nepal and other regions (Nuimura et al., 2012; Trüssel et al., 2013; King et al., 2017).

Widespread thinning of Himalayan glaciers has been revealed by differencing multitemporal DEMs constructed from  
65 satellite image photogrammetry (e.g., Gardelle et al., 2013; Maurer et al., 2016; Brun et al., 2017). Remote-sensing techniques  
(e.g., unmanned autonomous vehicle surveys) hold a key advantage over debris-covered glaciers, where the thinning also  
depends on variations in debris thickness and the spatial distribution of supraglacial ponds or ice cliffs (Vincent et al., 2016).  
Repeated differential GPS (DGPS) measurements, which are acquired with centimetre-scale accuracy, enable us to evaluate  
elevation changes of several metres (e.g., Fujita et al., 2008). Although their temporal and spatial coverage is limited, repeated  
70 DGPS measurements have been successfully acquired to investigate the surface elevation changes of debris-free glaciers in  
Bhutan (Tshering and Fujita, 2016) and the Inner Tien Shan (Fujita et al., 2011).

This study aims to quantify the contributions of ice dynamics and SMB to the thinning of adjacent land- and lake-  
terminating glaciers. To investigate the importance of glacial lake formation and expansion on glacier thinning, we measured  
surface elevation changes on lake- and land-terminating glaciers in the Lunana region, Bhutan Himalaya. Following a previous  
75 report of surface elevation measurements from a DGPS survey (Fujita et al., 2008), we repeated the DGPS survey on the lower  
parts of the land-terminating Thorthormi Glacier as well as the adjacent lake-terminating Lugge Glacier. Thorthormi and Lugge  
glaciers were selected for analysis because they are located at similar elevations. Lugge Glacier terminates in a proglacial lake,  
Lugge Glacial Lake, while the terminus of Thorthormi Glacier is grounded but a large supraglacial lake has developed in its  
ablation area (Bajracharya et al., 2014). These contrasting conditions make them suitable for evaluating the contribution of ice  
80 dynamics to the observed ice thickness changes. The glaciers are also suitable for field measurements because of their relatively  
safe ice-surface conditions and proximity to trekking routes. We also performed numerical simulations to evaluate the  
contributions of SMB and ice dynamics to surface elevation changes.

## 2 Study site

This study focuses on two debris-covered glaciers (Thorthormi and Lugge glaciers) in the Lunana region of northern Bhutan  
85 (Fig. 1a, 28°06' N, 90°18' E). Thorthormi Glacier covers an area of 13.16 km<sup>2</sup>, based on a satellite image from 17 January  
2010 (Table S1 in the Supplement, Nagai et al., 2016). The ice flows to the south in the upper part and to the southwest in the  
terminal part of the glacier at rates of 60–100 m a<sup>-1</sup> (Bolch et al., 2012). The surface is almost flat (< 1°) within 3000 m of the  
glacier terminus. The ablation area of the glacier thinned at a rate of -3 m a<sup>-1</sup> during the 2000–2010 period (Gardelle et al.,  
2013). A large supraglacial lake, which is inferred to possess a high potential for outburst flood (Fujita et al., 2008, 2013),  
90 formed on the western ablation area by the merging of multiple supraglacial ponds (Ageta et al., 2000; Komori, 2008).  
Thorthormi Glacier is termed a land-terminating glacier here since the glacier terminus was grounded in 2011.

Lugge Glacier is a lake-terminating glacier with an area of 10.93 km<sup>2</sup> in May 2010 (Table S1, Nagai et al., 2016). The  
mean surface slope is 12° within 3000 m of the glacier terminus. A moraine-dammed proglacial lake has expanded since the  
1960s (Ageta et al., 2000; Komori, 2008), and the glacier terminus retreated by ~1 km during 1990–2010 (Bajracharya et al.,

95 2014). Luge Glacier thinned near the terminus at a rate of  $-8 \text{ m a}^{-1}$  during 2000–2010 (Gardelle et al., 2013). On 7 October 1994, an outburst flood, with a volume of  $17.2 \times 10^6 \text{ m}^3$ , occurred from Luge Glacial Lake (Fujita et al., 2008). The depth of Luge Glacial Lake was 126 m at its deepest location, with a mean depth of 50 m, based on a bathymetric survey in September 2002 (Yamada et al., 2004).

100 Although the debris thickness was not measured during the field campaigns, there were regions of debris-free surface across the ablation areas of Thorthormi and Luge glaciers (Fig. S1 in the Supplement). Debris cover is therefore considered to be thin and sparse across the study area. Furthermore, few supraglacial ponds and ice cliffs were observed across Thorthormi and Luge glaciers.

105 Meteorological and glaciological in situ observations were acquired across the glaciers and lakes in the Lunana region from 2002 to 2004 (Yamada et al., 2004). Automatic weather station (AWS) observations from the terminal moraine of Luge Glacial Lake (4524 m a.s.l., Fig. 1a) showed that the annual mean air temperature during 2002–2004 was  $\sim 0 \text{ }^\circ\text{C}$ , and annual precipitation was 900 mm in 2003 (Suzuki et al., 2007b). Naito et al. (2012) reported changes in surface elevation and ice flow velocity along the central flowline in the lower parts of Thorthormi and Luge glaciers for the 2002–2004 period. The ice thinning rate at Luge Glacier was  $\sim 5 \text{ m a}^{-1}$  during 2002–2004, which is much higher than that at Thorthormi Glacier ( $0\text{--}3 \text{ m a}^{-1}$ ). The surface flow velocities of Thorthormi Glacier decrease down-glacier from  $\sim 90$  to  $\sim 30 \text{ m a}^{-1}$  at 2000–3000 m from 110 the terminus, while the surface flow velocities of Luge Glacier are nearly uniform at  $40\text{--}55 \text{ m a}^{-1}$  within 1500 m of the terminus (Naito et al., 2012).

### 3 Data and methods

#### 3.1 Surface elevation change

115 We surveyed the surface elevations in the lower parts of Thorthormi and Luge glaciers from 19 to 22 September 2011, and then compared them with those observed from 29 September to 10 October 2004 (Fujita et al., 2008). We used dual- and single-frequency carrier phase GPS receivers (GNSS Technologies, GEM-1, and MAGELLAN ProMark3). One receiver was installed 2.5 km west of the terminus of Thorthormi Glacier as a reference station (Fig. 1a), whose location was determined by an online precise point positioning processing service (<https://webapp.geod.nrcan.gc.ca/geod/tools-outils/ppp.php?locale=en>, last accessed: 31 May 2018), which provided standard deviations of  $< 4 \text{ mm}$  for both the horizontal and vertical coordinates after one week of continuous measurements in 2011. Observers walked on/around the glaciers with a 120 GPS receiver and antenna fixed to a frame pack. The height uncertainty of the GPS antenna during the survey was  $< 0.1 \text{ m}$  (Tsutaki et al., 2016). We neglected the influence of debris cover on changes in the GPS antenna height because the debris cover across the glaciers is sparse and thin, and we therefore could walk on the ice surface across most of the surveyed area. The GPS data were processed with RTKLIB, an open source software for GNSS positioning (<http://www.rtklib.com/>, last 125 accessed: 31 May 2018). Coordinates were projected onto a common Universal Transverse Mercator projection (UTM zone 46N, WGS84 reference system). We generated DEMs with 1 m resolution by interpolating the surveyed points with an inverse

distance weighted method, as used in previous studies (e.g., Fujita and Nuimura, 2011; Tshering and Fujita, 2016). The 2004 survey data were calibrated with four benchmarks around the glaciers (Fig. 1a) to generate a 1 m resolution DEM. Details of the 2004 and 2011 GPS surveys, along with their respective DEMs, are summarised in Table S1. The surface elevation changes  
130 between 2004 and 2011 were computed at points where data were available for both dates. Elevation changes were obtained at 431 and 248 DEM grid points for Thorthormi and Lugge glaciers, respectively (Table 1).

The horizontal uncertainty of the GPS survey was evaluated by comparing the positions of four benchmarks installed around Lugge and Thorthormi glaciers (Fig. 1a). We evaluated the vertical uncertainty ( $\sigma_e$ ) from the off-glacier elevation difference between the 2004 and 2011 DEMs ( $n = 3893$ , Table 1), which was calculated as the quadratic sum of the mean elevation  
135 difference ( $dZ$ ) and standard deviation ( $\sigma_z$ ) (Bolch et al., 2011). In previous studies, the vertical uncertainty in differentiation of two satellite-based DEMs has been expressed by the standard error ( $\sigma_{se}$ ) as follows:

$$\sigma_{se} = \frac{\sigma_e}{\sqrt{n}}. \quad (1)$$

140 The number of DEM grid points over a glacier is generally used as the sample number  $n$  (e.g., Berthier et al., 2007; Bolch et al., 2011; Maurer et al., 2016).

To evaluate the spatial representativeness of the change in glacier surface elevation change derived from DGPS measurements, we compared the elevation changes derived from the DGPS-DEMs and Advanced Spaceborne Thermal Emission and Reflection Radiometer (ASTER) DEMs acquired on 11 October 2004 and 6 April 2011, respectively, which  
145 cover a similar period to our field campaigns (2004–2011). The 30 m ASTER-DEMs were provided by the ASTER-VA (<https://gbank.gsj.jp/madas/map/index.html>, last accessed: 31 May 2018) and used to compute the surface elevation change. The ASTER-DEM elevations were calibrated using the DGPS data on the ice-free terrain in 2011. The 2004 and 2011 ASTER-DEMs had positive biases of 12.73 and 11.20 m, and standard deviations of 20.24 and 14.04 m, respectively. The vertical coordinates of the ASTER-DEMs were then corrected for the corresponding bias, with the elevation change over the glacier  
150 surface computed as the difference between the calibrated DEMs.

### 3.2 Surface flow velocities

We calculated surface flow velocities by processing ASTER images (15 m resolution, near infrared (NIR), near nadir 3N band) with the COSI-Corr feature tracking software (Leprince et al., 2007), which is commonly adopted in mountainous terrain to measure surface displacements with an accuracy of one-fourth to one-tenth of the pixel size (e.g., Heid and Kääb, 2012;  
155 Scherler and Strecker, 2012; Lamsal et al., 2017). Orthorectification and coregistration of the images were performed by Japan Space Systems before processing. The orthorectification and coregistration accuracies were reported as 16.9 m and 0.05 pixel, respectively. We selected five image pairs from seven scenes between 22 October 2002 and 12 October 2010, with temporal separations ranging from 273 to 712 days (Table S2), to obtain annual surface flow velocities of the glaciers. It should be noted

that the aim of our flow velocity measurements is to investigate the mean surface flow regime of the glaciers rather than its  
160 interannual variability. The subpixel displacement of features on the glacier surface was recorded at every fourth pixel in the  
orthorectified ASTER images, providing the horizontal flow velocities at a 60 m resolution (Scherler et al., 2011b). We used  
a statistical correlation mode, with a correlation window size of  $16 \times 16$  pixels (Leprince et al., 2007). We applied a filter with  
a signal to noise ratio threshold of  $< 0.9$ . The obtained ice flow velocity fields were filtered to remove residual attitude effects  
and miscorrelations (Scherler et al., 2011b; Scherler and Strecker, 2012). The filters eliminated those flow vectors showing a  
165 large deviation in magnitude (greater than  $\pm 1 \sigma$ ) or direction ( $> 20^\circ$ ) relative to the mean of the neighbouring  $21 \times 21$  data  
points.

### 3.3 Glacier area

We analysed the areal variations in the ablation area of Thorthormi and Lugge glaciers using 12 satellite images acquired by  
the Landsat 7 ETM+ between November 2000 and December 2011 (distributed by the United States Geological Survey,  
170 <http://landsat.usgs.gov/>, last accessed: 31 May 2018). We selected images taken in either November or December with the  
least snow and cloud cover. We also analysed multiple ETM+ images acquired from the October to December timeframe of  
each year to avoid the scan line corrector-off gaps. The lowermost 4000 m of Thorthormi Glacier and the lowermost 2000 m  
of Lugge Glacier were manually delineated on false colour composite images (bands 3–5, 30 m spatial resolution) in a  
geographical information system. Following to the previously proposed delineation methods (e.g., Bajracharya et al., 2014;  
175 Nuimura et al., 2015; Nagai et al., 2016), supraglacial ponds surrounded by ice were included in the glacier surface, whereas  
marginal ponds in contact with bedrock/moraine ridge were excluded. The accuracy of the outline mapping is equivalent to  
the image resolution (30 m). The coregistration error in the repeated images was  $\pm 30$  m, based on visual inspection of the  
horizontal shift of a stable bedrock and lateral moraines on the coregistered imagery. The user-induced error was estimated to  
be 5 % of the glacier area delineated from the Landsat images (Paul et al., 2013). The total error of the area analysis was  $\pm 0.17$   
180 and  $\pm 0.05$  km<sup>2</sup> for Thorthormi and Lugge glaciers, respectively.

### 3.4 Mass balance of the debris-covered surface

SMB is an essential component of ice thickness change, but no in situ SMB data are available in the Lunana region. Therefore,  
the spatial distributions of the SMB on the debris-covered Thorthormi and Lugge glaciers were computed with a heat and mass  
balance model, which quantifies the spatial distribution of the mean SMB for each glacier.

185 Thin debris accelerates ice melt by lowering surface albedo, while thick debris (generally more than a few centimetres)  
suppresses ice melt and acts as an insulating layer (Østrem, 1959; Mattson et al., 1993). To obtain the spatial distributions of  
debris thickness and SMB, we estimated the thermal resistance from remotely sensed data and reanalysis climate data (Suzuki  
et al., 2007a; Zhang et al., 2011; Fujita and Sakai, 2014). The thermal resistance ( $R_T$ , m<sup>2</sup> K W<sup>-1</sup>) is defined as follows:

$$190 \quad R_T = \frac{h}{\lambda}, \quad (2)$$

where  $h$  and  $\lambda$  are debris thickness (m) and thermal conductivity ( $\text{W m}^{-1} \text{K}^{-1}$ ), respectively. This method has been applied to reproduce debris thickness and SMB in southeastern Tibet (Zhang et al., 2011) and glacier runoff in the Nepal Himalaya (Fujita and Sakai, 2014). Assuming no heat storage, a linear temperature profile within the debris layer, and the melting point  
 195 temperature at the ice–debris interface ( $T_i$ , 0 °C), the conductive heat flux through the debris layer ( $G_d$ ,  $\text{W m}^{-2}$ ) and the heat balance at the debris surface are described as follows:

$$G_d = \frac{(T_s - T_i)}{R_T} = (1 - \alpha_d)R_{sd} + R_{ld} - R_{lu} + H_s + H_l, \quad (3)$$

200 where  $\alpha_d$  is the debris surface albedo;  $R_{sd}$ ,  $R_{ld}$ , and  $R_{lu}$  are the downward short wave radiation, and downward and upward long wave radiation, respectively (positive sign,  $\text{W m}^{-2}$ ); and  $H_s$  and  $H_l$  are the sensible and latent heat fluxes ( $\text{W m}^{-2}$ ), respectively, which are positive when the fluxes are directed toward the ground. Both turbulent fluxes were ignored in the original method to obtain the thermal resistance based on a sensitivity analysis and field measurements (Suzuki et al., 2007a). However, we improved the method by taking the sensible heat into account because several studies have indicated that ignoring  
 205 the sensible heat can result in an underestimation of the thermal resistance (e.g., Reid and Brock, 2010). Using eight ASTER images obtained between October 2002 and October 2010 (Table S3), along with the NCEP/NCAR reanalysis climate data (NCEP-2, Kanamitsu et al., 2002), we calculated the distribution of mean thermal resistance on the two target glaciers. The air temperature at the AWS elevation (4524 m a.s.l., Fig. 1a) was estimated using the pressure level atmospheric temperature and geopotential height (Sakai et al., 2015), and then modified for each  $90 \times 90$  m mesh grid points using a single temperature  
 210 lapse rate ( $0.006 \text{ }^\circ\text{C km}^{-1}$ ). The wind speed was assumed to be  $2.0 \text{ m d}^{-1}$ , which is the two-years average of the 2002–2004 AWS record (Suzuki et al., 2007b). The uncertainties in the thermal resistance and albedo were evaluated as 107 and 40 %, respectively, by taking the standard deviations calculated from multiple images at the same location (Fig. S2).

The SMB of the debris-covered ablation area was calculated by a heat and mass balance model that included debris-covered effects (Fujita and Sakai, 2014). First, the surface temperature is determined to satisfy Eq. (3) using the estimated thermal  
 215 resistance and an iterative calculation, and then, if the heat flux toward the ice–debris interface is positive, the daily amount of ice melt beneath the debris mantle ( $M_d$ ,  $\text{kg m}^{-2} \text{d}^{-1}$ ) is obtained as follows:

$$M_d = \frac{t_D G_d}{l_m}, \quad (4)$$

$$220 \quad b = c + \left( \sum_{D=1}^{365} \frac{t_D H_L}{l_m} - D_S - M_d \right) / 1000 \quad (5)$$

where  $t_D$  is the length of a day in seconds (86400 s), and  $l_m$  is the latent heat of fusion of ice ( $3.33 \times 10^5 \text{ J kg}^{-1}$ ),  $b$  and  $c$  are annual mass balance and accumulation (m w.e.  $\text{a}^{-1}$ ), respectively, and  $D_S$  is the daily discharge ( $\text{kg m}^{-2} \text{ d}^{-1}$ ). Further details on the equations and methodology used in the model are described by Fujita and Sakai (2014). The mass balance was calculated at  $90 \times 90$  m mesh grid points on the ablation area of the two glaciers using 38 years of ERA-Interim reanalysis data (1979–2017), with the results given in metres of water equivalent (w.e.). The meteorological variables in the ERA-Interim reanalysis data (2002–2004) were calibrated with in situ meteorological data (2002–2004) from the terminal moraine of Lugge Glacier (Fig. S3). The ERA-Interim wind speed was simply multiplied by 1.3 to obtain the same average as in the observational data. The SMBs calculated with the observed and calibrated ERA-Interim data for 2002–2004 were compared with those from the entire 38-year ERA-Interim data set. The SMBs for 2002–2004 (from both the observational and ERA-Interim data sets) show no clear anomaly against the long-term mean SMB (1979–2017) (Fig. S4).

The sensitivity of the simulated meltwater was evaluated against the meteorological parameters used in the SMB model. We chose meltwater instead of SMB to quantify the uncertainty because the SMB uncertainty cannot be evaluated as absolute value. The tested parameters are surface albedo, air temperature, precipitation, relative humidity, solar radiation, thermal resistance and wind speed. The thermal resistance and albedo uncertainties were based on the standard deviations derived from the eight ASTER images used to estimate these parameters (Fig. S2). Each meteorological variable uncertainty, with the exceptions of the thermal resistance and albedo uncertainties, was assumed to be the root mean square error (RMSE) of the ERA-Interim reanalysis data against the observational data (Fig. S3). The simulated meltwater uncertainty was estimated as the variation in meltwater within a possible parameter range via a quadratic sum of the results from each meteorological parameter.

### 3.5 Ice dynamics

#### 3.5.1 Model descriptions

To investigate the dynamically induced ice thickness change, numerical experiments were carried out by applying a two-dimensional ice flow model to the longitudinal cross sections of Thorthormi and Lugge glaciers. The aim of the experiments was to investigate whether the ice thickness changes observed at Thorthormi and Lugge glaciers were affected by the presence of proglacial lakes.

The model was developed for a land-terminating glacier (Sugiyama et al., 2003, 2014), and is applied to the lake-terminating glaciers in this study. Taking the  $x$  and  $z$  coordinates in the along flow and vertical directions, the momentum and mass conservation equations in the  $x$ – $z$  plane are:

$$\frac{\partial \sigma_{xx}}{\partial x} + \frac{\partial \sigma_{xz}}{\partial z} = 0, \quad (6)$$

$$\frac{\partial \sigma_{zx}}{\partial x} + \frac{\partial \sigma_{zz}}{\partial z} = \rho_i g, \quad (7)$$

$$255 \quad \frac{\partial u_x}{\partial x} + \frac{\partial u_z}{\partial z} = 0, \quad (8)$$

where  $\sigma_{ij}$  ( $i, j = x, z$ ) are components of the Cauchy stress tensor,  $\rho_i$  is the density of ice ( $910 \text{ kg m}^{-3}$ ),  $g$  is the vertical component of the gravitational acceleration vector ( $9.81 \text{ m s}^{-2}$ ), and  $u_x$  and  $u_z$  are the horizontal and vertical components of the flow velocity vector, respectively. The stress in Eqs. (7) and (8) is linked to the strain rate via the constitutive equation given by  
 260 Glen's flow law (Glen, 1955):

$$\dot{\epsilon}_{ij} = A \tau_e^{n-1} \tau_{ij}, \quad (9)$$

where  $\dot{\epsilon}_{ij}$  and  $\tau_{ij}$  are the components of the strain rate and deviatoric stress tensors, respectively, and  $\tau_e$  is the effective stress,  
 265 which is described as

$$\tau_e = \frac{1}{2} (\tau_{xx}^2 + \tau_{zz}^2) + \tau_{xz}^2. \quad (10)$$

The rate factor ( $A$ ) and flow law exponent ( $n$ ) are material parameters. We used the commonly accepted value of  $n = 3$  for the  
 270 flow law exponent and employed a rate factor of  $A = 75 \text{ MPa}^{-3} \text{ a}^{-1}$ , which was previously used to model a temperate valley glacier (Gudmundsson, 1999). We assumed the glaciers were temperate because there was no available information on the thermal states of the studied glaciers.

The model domain was within 5100 m and 3500 m from the terminus of Thorthormi (red and white lines in Fig. 1b) and  
 275 Lugge glaciers (red line in Fig. 1b), respectively. The surface elevation of the model domain ranges from 4442 to 4813 m for Thorthormi Glacier, and from 4530 to 5244 m for Lugge Glacier. The surface geometry was obtained from ASTER GDEM version 2 after filtering the elevations with a smoothing routine at a bandwidth of 1000 m. The ice thickness distribution was estimated from a method proposed for alpine glaciers (Farinotti et al., 2009). We applied the same local regression filter to smooth the estimated bedrock geometry. The bedrock elevation of Thorthormi Glacier was estimated from bathymetry data acquired in September 2011 at 1400 m from the terminus. For Lugge Glacier, the bed elevation at the glacier front was  
 280 estimated from the bathymetric map of Lugge Glacial Lake, surveyed in September 2002 (Yamada et al., 2004). To solve Eqs. (7) and (8) for  $u_x$  and  $u_z$ , the modelled domain was discretised with a finite element mesh. The mesh resolution was 100 m in the horizontal direction, and several metres near the bed and 10–28 m near the surface in the vertical direction. The total numbers of elements were 612 and 420 for Thorthormi and Lugge glaciers, respectively.

The upper surface of the domain was assumed to be stress free. The ice flux through the upper boundary was prescribed according to the measured surface flow velocities. The basal sliding velocity ( $u_b$ ) was given as a linear function of the basal shear traction ( $\tau_{xz,b}$ ):

$$u_b = C\tau_{xz,b} , \quad (11)$$

where  $C$  is the sliding coefficient. We used constant sliding coefficients of  $C = 766$  and  $125 \text{ m a}^{-1} \text{ MPa}^{-1}$  over the entire domains of Thorthormi and Lugge glaciers, respectively. These parameters were obtained by minimising the RMSE between the modelled and measured surface flow velocities over the entire model domains (Fig. S5).

### 3.5.2 Experimental configurations

To quantify the effect of glacier dynamics on ice thickness change, we performed two experiments for Thorthormi and Lugge glaciers. Experiment 1 was performed to compute the ice flow velocity fields under the present terminus conditions. In this experiment, Thorthormi Glacier was treated as a land-terminating glacier by prescribing zero horizontal velocity at the glacier front, whereas Lugge Glacier was treated as a lake-terminating glacier by applying hydrostatic pressure at the front as a function of water depth. A stress-free boundary condition was given to the calving front above the lake level.

Experiment 2 was designed to investigate the influence of proglacial lakes on glacier dynamics. For Thorthormi Glacier, we assumed a calving front with thickness of 106 m (red line in Fig. 1b). The surface level of the proglacial lake was assumed to be 4432 m a.s.l., which is the mean surface level of the supraglacial ponds measured in September 2004 (Fujita et al., 2008). Hydrostatic pressure and stress-free conditions were applied to the lower boundary below and above the lake level, respectively. For Lugge Glacier, we simulated a lake-free situation, with ice flowing to the contemporary terminal moraine, so that the glacier terminates on land. Bedrock topography is derived from the bathymetric map (red and white lines in Fig. 1b, Yamada et al., 2004). The surface topography is linearly extrapolated from the surface elevations at the calving front in 2002, and zero flow velocity was assumed at the terminus. In the experiment, we used 444 and 684 elements for Thorthormi and Lugge glaciers, respectively.

### 3.6 Simulated ice thickness change

To compare the influence of ice dynamics on glacier thinning in lake- and land-terminating glaciers, we calculated the emergence velocity ( $v_e$ ) as follows:

$$v_e = (v_z - v_h \tan \alpha) \frac{\rho_i}{\rho_w} , \quad (12)$$

where  $v_z$  and  $v_h$  are the vertical and horizontal flow velocities, respectively, and  $\alpha$  is the surface slope (Cuffey and Paterson, 2010). The surface slope  $\alpha$  was obtained every 100 m from the surface topography of the ice flow model. The emergence velocity was converted to water equivalent (m w.e. a<sup>-1</sup>), using the densities of ice ( $\rho_i$ , 910 kg m<sup>-3</sup>) and water ( $\rho_w$ , 1000 kg m<sup>-3</sup>), for comparison with the SMB. The surface elevation change over time ( $dh/dt$ , m a<sup>-1</sup>), which is caused by the imbalance of the emergence velocity and SMB ( $b$ ) along the central flowline, is calculated as

$$320 \quad \frac{dh}{dt} = (b + v_e) \frac{\rho_w}{\rho_i} . \quad (13)$$

The magnitude of the emergence velocity is approximately proportional to the horizontal flow velocity (Truffer et al., 2009). Assuming this relationship, the emergence velocity uncertainty ( $\sigma_{ve}$ ) was estimated as

$$325 \quad \sigma_{ve} = \frac{v_e}{u_{model}} \times \sigma_{u_{model}} , \quad (14)$$

where  $u_{model}$  is the simulated horizontal flow velocity and  $\sigma_{u_{model}}$  is the mean uncertainty of the simulated surface flow velocity.

## 4 Results

### 330 4.1 Surface elevation change

Figure 1a shows the rate of surface elevation change of Thorthormi and Lugge glaciers from 2004 to 2011. The rates for Thorthormi Glacier range from  $-3.37$  to  $+1.14$  m a<sup>-1</sup>, with a mean rate of  $-1.40$  m a<sup>-1</sup> (Table 1). These rates show large variability within the limited elevation band (4410–4450 m a.s.l., Fig. 2b). No clear trend is observed at 1000–3000 m from the terminus (Fig. 2c). The rates for Lugge Glacier range from  $-9.13$  to  $-1.30$  m a<sup>-1</sup>, with a mean rate of  $-4.67$  m a<sup>-1</sup> (Table 1). The most negative values ( $-9$  m a<sup>-1</sup>) are found in the lower elevation band (4560 m a.s.l., Fig. 2b), which corresponds to 1300 m from the 2002 terminus position (Fig. 2c).

The RMSE between the surveyed positions (five measurements in total, with one or two measurements for each benchmark) is 0.21 m in the horizontal direction. The mean elevation difference between the 2004 and 2011 DEMs ( $dZ$ ) is 0.48 m, with a standard deviation ( $\sigma_z$ ) of 1.91 m (Fig. 2a) and a vertical uncertainty ( $\sigma_e$ ) is 1.97 m (0.28 m a<sup>-1</sup>). According to Eq. (1), the standard error for this study ranges from 0.09 to 0.12 m ( $\sim 0.02$  m a<sup>-1</sup>), while those for the remotely sensed studies of Himalayan glaciers have been evaluated at 1.1–6.4 m (e.g., Berthier et al., 2007; Bolch et al., 2011; Maurer et al., 2016), suggesting that our data are considerably more accurate than those reported in the aforementioned studies.

Given the ASTER-DEM uncertainties, the DGPS-DEMs and ASTER-DEMs yield a similar rate of elevation change that falls within the uncertainty range (Fig. S6). The mean rates of elevation change, with their respective standard deviations, from the DGPS-DEMs are  $-1.40 \pm 0.77$  and  $-4.67 \pm 1.36$  m a<sup>-1</sup> for Thorthormi and Lugge glaciers, respectively, while those from the ASTER-DEMs over the same elevation range as the DGPS measurements are  $-0.70 \pm 1.25$  and  $-4.87 \pm 1.29$  m a<sup>-1</sup>, respectively. The DGPS-DEM rates are in good agreement with the ASTER-DEM rates (Fig. S7), thus supporting the applicability of the DGPS measurements to the entire ablation area.

#### 4.2 Surface flow velocities

Figure 1b shows the surface flow velocity field from 30 January 2007 to 1 January 2008 (337 days). On Thorthormi Glacier, the flow velocities decrease down-glacier, ranging from  $\sim 110$  m a<sup>-1</sup> at the foot of the icefall to  $< 10$  m a<sup>-1</sup> at the terminus (Fig. 3a). The flow velocities of Lugge Glacier increase down-glacier, ranging from 20–60 to 50–80 m a<sup>-1</sup> within 2000 m of the calving front (Fig. 3b). In this region, the ice flow converges as the glacier width narrows down-glacier. The flow velocity uncertainty was estimated to be 12.1 m a<sup>-1</sup>, as given by the mean off-glacier displacement from 3 February 2006 to 30 January 2007 (0.99 years) (Fig. S8).

#### 4.3 Changes in glacier terminus

Thorthormi Glacier progressively shrank in size from 2000 to 2010, at a mean rate of  $-0.09$  km<sup>2</sup> a<sup>-1</sup> and accelerated loss between 2010 and 2011 ( $-0.49$  km<sup>2</sup> a<sup>-1</sup>) (Figs. 4a and 5). This change was due to the rapid retreat of the northern half of the glacier front by 200–1400 m. Lugge Glacier also shrank in size from 2000 to 2011, at a mean rate of  $-0.03$  km<sup>2</sup> a<sup>-1</sup> (Figs. 4b and 5). Since 2009, the calving front has retreated more rapidly along the northern half of the glacier front (by 300–400 m) than along the southern half (by  $< 200$  m) (Fig. 4b). The total area changes from 2000 to 2011 are  $-1.40$  km<sup>2</sup> and  $-0.33$  km<sup>2</sup> for Thorthormi and Lugge glaciers, respectively.

#### 4.4 Mass balance of the debris-covered surface

The simulated SMB shows a spatially heterogeneous distribution between the two glaciers (Fig. 1c). For example, the SMB ranges from  $-9.5$  to  $-2.0$  m w.e. a<sup>-1</sup>, with a mean rate of  $-7.4 \pm 0.1$  m w.e. a<sup>-1</sup>, over the simulated region of Thorthormi Glacier. For Lugge Glacier, the SMB ranges from  $-8.7$  to  $-0.9$  m w.e. a<sup>-1</sup>, with a mean rate of  $-5.3 \pm 0.1$  m w.e. a<sup>-1</sup>. The mean SMB is  $-9.0 \pm 0.1$  and  $-6.7 \pm 0.2$  m w.e. a<sup>-1</sup> across the DGPS survey area of Thorthormi and Lugge glaciers, respectively (Table 1). The debris-free surface has a more negative SMB than the debris-covered regions of the glaciers. The mean SMB over the simulated region of Thorthormi Glacier is  $-9.3 \pm 0.7$  and  $-7.3 \pm 0.1$  m w.e. a<sup>-1</sup> on the debris-free and debris-covered surfaces,

370 respectively. The mean SMB of Luge Glacier is  $-7.3 \pm 0.4$  m w.e.  $a^{-1}$  and  $-5.4 \pm 0.2$  m w.e.  $a^{-1}$  on the debris-free and debris-covered surfaces, respectively.

The sensitivity of simulated meltwater in the SMB model was evaluated as a function of the RMSE of each meteorological variable across the debris-covered area (Fig. S9). Ice melting is more sensitive to solar radiation and thermal resistance. The influence of thermal resistance on meltwater formation is considered to be small since the debris cover is thin and sparse over  
375 the glaciers. The estimated meltwater uncertainty is  $< 50$  % across most of Thorthormi and Luge glaciers (Fig. S10).

#### 4.5 Numerical experiments of ice dynamics

The ice thinning of Luge Glacier was three times faster than that of Thorthormi Glacier. However, the mean SMB was 1.4 times more negative at Thorthormi Glacier, suggesting a substantial influence of glacier dynamics on ice thickness change. To quantify the contribution of ice dynamics to the ice thickness change, we performed numerical experiments with the present  
380 (Experiment 1) and prescribed (Experiment 2) glacier geometries.

##### 4.5.1 Experiment 1 – present geometry

Modelled results for the present geometry show significantly different flow velocity fields for Thorthormi and Luge glaciers (Figs. 6c and 6d). Thorthormi Glacier flows faster ( $> 150$  m  $a^{-1}$ ) in the upper reaches, where the surface is steeper than the other regions (Fig. 6c). Down-glacier of the icefall, where the glacier surface is flatter, the ice motion slows in the down-glacier direction, with the flow velocities decreasing to  $< 10$  m  $a^{-1}$  near the terminus (Fig. 6e). Ice flows upward relative to the  
385 surface across most of the modelled region (Fig. 6c). In contrasted to the observed decrease in the flow velocities at Thorthormi, the computed flow velocities of Luge Glacier gradually increase down-glacier, up to  $\sim 40$  m  $a^{-1}$ , and then sharply increase to  $\sim 80$  m  $a^{-1}$  at the calving front (Fig. 6f). Ice flow is nearly parallel to the glacier surface, except for the more downward motion near the calving front (Fig. 6d). Within 3000 m of the terminus of Thorthormi Glacier, the modelled surface flow velocities  
390 are in good agreement with the satellite-derived flow velocities (Fig. 6e). The calculated surface flow velocities of Luge Glacier are within 7 % of the satellite-derived flow velocities (Fig. 6f).

##### 4.5.2 Experiment 2 – contrasting geometry

Figure 7c shows the flow velocities simulated for the lake-terminating boundary condition of Thorthormi Glacier, in which the flow velocities within 200 m of the calving front are three to four times faster than those of Experiment 1 (Figs. 6c and 7c).  
395 The mean vertical surface flow velocity within 2000 m of the front is still positive ( $0.9$  m  $a^{-1}$ ), but is smaller than that for the land-terminating condition ( $1.6$  m  $a^{-1}$ ). The modelled result demonstrates significant acceleration as the glacier dynamics change from a compressive to stretching flow regime after proglacial lake formation. For Luge Glacier, the flow velocities decrease over the entire glacier in comparison with Experiment 1 (Figs. 6d and 7d). The upward ice motion appears within

3000 m of the terminus. The numerical experiments demonstrate that the formation of a proglacial lake causes significant changes in ice dynamics.

#### 4.5.3 Simulated surface flow velocity uncertainty

Although we assumed Thorthormi and Lugge glaciers were temperate in the model, the simulated ice flow is mostly due to basal sliding in the ablation area of both glaciers (Figs. 6e and 6f). The influence of this assumption on the flow velocity computations is therefore small because our model indicated moderate ice deformation in the glaciers. The RMSEs between the modelled and measured flow velocities were computed as a measure of the model performance (Fig. S5). For Thorthormi Glacier, the model exhibits similar sensitivities to the sliding coefficient and ice thickness. For Lugge Glacier, the model is more sensitive to the ice thickness than the sliding coefficient. Sensitivity tests demonstrate that the simulated surface flow velocities of Thorthormi Glacier vary by  $\pm 30\%$  when the constant sliding coefficient ( $C$ ) and ice thickness are varied by  $\pm 30\%$  (Fig. S11). For Lugge Glacier, the simulated flow velocities vary by 22 and 65 % when the sliding coefficient and ice thickness are varied by  $\pm 30\%$ , respectively. The simulated surface flow velocity uncertainty is estimated as the quadratic sum of the accuracy of the surface flow velocity measurements, interannual variability in the measured surface flow velocities and the RMSE between the modelled and measured surface flow velocities. The mean uncertainty of the simulated surface flow velocity ( $\sigma_{u,model}$ ) is 20.7 and 26.9 m a<sup>-1</sup> for Thorthormi and Lugge glaciers, respectively.

#### 4.6 Simulated ice thickness change

Figure 8a shows the computed emergence velocity and SMB along the central flowlines of the glaciers. Given the computed surface flow velocities from Experiment 1, the emergence velocity of Lugge Glacier ranges from  $-1.3$  to  $0.3$  m w.e. a<sup>-1</sup>, with a mean value of  $-0.2 \pm 0.1$  m w.e. a<sup>-1</sup> within 700–1500 m of the terminus (Fig. 8a) and more negative values near the calving front, reaching approximately  $-10$  m w.e. a<sup>-1</sup> due to the increase in surface flow velocities toward the glacier front (Fig. 6f). In contrast to Lugge Glacier, the emergence velocity of Thorthormi Glacier is positive over the entire model domain, ranging from 1.9 to 5.4 m w.e. a<sup>-1</sup>, with a mean value of  $3.1 \pm 0.4$  m w.e. a<sup>-1</sup> within 1300–2800 m of the terminus that increases to  $> 10$  m a<sup>-1</sup> in the upper reaches of the glacier (Fig. 8a).

The emergence velocity computed under contrasting geometries (Experiment 2) varies from that with the present geometries (Experiment 1) for both Thorthormi and Lugge glaciers. For the land-terminating condition of Lugge Glacier, the mean emergence velocity is positive ( $1.4 \pm 0.1$  m w.e. a<sup>-1</sup>) within 700–1500 m of the terminus. The mean emergence velocity of Thorthormi Glacier computed with the lake-terminating condition is  $1.8 \pm 0.4$  m w.e. a<sup>-1</sup> within 1300–2800 m of the terminus, which decreases by 42 % from the land-terminating condition.

Under the modelled conditions of Experiment 1, the computed rate of elevation change of Lugge Glacier is  $-9.0$  to  $-5.2$   $\text{m a}^{-1}$ , with a mean rate of  $-7.7 \pm 0.7$   $\text{m a}^{-1}$  within 700–1500 m from the calving front, which is 61 % more negative than the observations (Fig. 8). For Thorthormi Glacier, the rate of elevation change ranges from  $-7.1$  to  $-4.1$   $\text{m a}^{-1}$ , with a mean rate of  
430  $-6.1 \pm 0.9$   $\text{m a}^{-1}$  over the in situ surveyed domain (Fig. 8). These values agree with the observations that were made 2400–3200 m from the terminus, falling within the uncertainty range, whereas they are much more negative than the observations along the lower reaches of the glacier.

Given the same SMB distribution of Experiment 1, the mean rate of elevation change was computed as  $-7.4 \pm 1.0$   $\text{m a}^{-1}$  (1300–2800 m) for Thorthormi Glacier with the lake-terminating condition and  $-6.0 \pm 0.8$   $\text{m a}^{-1}$  (1300–2800 m) for the land-  
435 terminating Lugge Glacier.

The mean uncertainty of the emergence velocity is 2.0 and 1.7  $\text{m w.e. a}^{-1}$  for Thorthormi and Lugge glaciers, respectively. The uncertainty of the computed rate of elevation change is estimated to be 2.4 to 8.3  $\text{m a}^{-1}$  for Thorthormi Glacier and 1.6 to 8.3  $\text{m a}^{-1}$  for Lugge Glacier.

## 5 Discussion

### 440 5.1 Glacier thinning

The repeated GPS surveys revealed rapid thinning of Lugge Glacier between 2004 and 2011. The mean rate of surface elevation change ( $-4.67 \pm 0.02$   $\text{m a}^{-1}$ ) is comparable to that for 2002–2004 period ( $-5$   $\text{m a}^{-1}$ , Naito et al., 2012). Gardelle et al. (2013) reported the rates of surface elevation change ranging from  $-8$  to  $-3$   $\text{m a}^{-1}$  during 2000–2010, as determined from the differencing of satellite-derived DEMs. Lugge Glacier is thinning more rapidly than neighbouring glaciers in the Nepal and  
445 Bhutan Himalayas. The mean rate of surface elevation change was  $-0.50 \pm 0.14$   $\text{m a}^{-1}$  in the ablation area of Bhutanese glaciers for the period 2000–2010 (Gardelle et al., 2013), and  $-2.30 \pm 0.53$   $\text{m a}^{-1}$  for debris-free glaciers in eastern Nepal and Bhutan during 2003–2009 (Kääb et al., 2012). Maurer et al. (2016) reported that the mean thinning rate for Lugge Glacier during 1974–2006 ( $-0.6 \pm 0.2$   $\text{m a}^{-1}$ ) was greater than those for other Bhutanese lake-terminating glaciers ( $-0.2$  to  $-0.4$   $\text{m a}^{-1}$ ). The rate of surface elevation change of Thorthormi Glacier (from  $-3.37$  to  $+1.14$   $\text{m a}^{-1}$  from 2004 to 2011) is comparable with  
450 previous measurements, which range from  $-3$  to  $0$   $\text{m a}^{-1}$  for the period 2002–2004 (Naito et al., 2012) and from  $-3$  to  $0$   $\text{m a}^{-1}$  during 2000–2010 (Gardelle et al., 2013). The mean rate across Thorthormi Glacier was  $-0.3 \pm 0.2$   $\text{m a}^{-1}$  during 1974–2006 (Maurer et al., 2016), which is a typical rate in the Bhutan Himalaya.

Lugge Glacier thinned more rapidly than Thorthormi Glacier, which is consistent with previous satellite-based studies. For example, the thinning rates of the lake-terminating Imja and Lumding glaciers ( $-1.14$  and  $-3.41$   $\text{m a}^{-1}$ , respectively) were  $\sim 4$   
455 times greater than those of the land-terminating glaciers (approximately  $-0.87$   $\text{m a}^{-1}$ ) in the Khumbu region of the Nepal

Himalaya (Nuimura et al., 2012). King et al. (2017) measured the thinning of the lower parts of nine lake-terminating glaciers in the Everest area (approximately  $-2.5 \text{ m a}^{-1}$ ), which was 67 % faster than that of 18 land-terminating glaciers (approximately  $-1.5 \text{ m a}^{-1}$ ). The lake-terminating glaciers in Yakutat ice field, Alaska, thinned at a rate of  $-4.76 \text{ m a}^{-1}$ , which was  $\sim 30$  % greater than the neighbouring land-terminating glaciers (Trüssel et al., 2013). It should be noted that the difference in thinning rate between Lugge and Thorthormi glaciers (3.3 times) is much greater than the numbers previously reported in the Nepal Himalaya, suggesting that ice dynamics play a more significant role here.

Glacier thinning has accelerated from 1970s to 2000s, particularly in the lower parts of Lugge and Thorthormi glaciers. For example, the mean rates of elevation change over Lugge ( $-4.67 \pm 0.02 \text{ m a}^{-1}$ ) and Thorthormi ( $-1.40 \pm 0.01 \text{ m a}^{-1}$ ) are more negative than those reported for the 1974–2006 period ( $-1.7 \pm 0.2 \text{ m a}^{-1}$  for Lugge and  $-0.9 \pm 0.2 \text{ m a}^{-1}$  for Thorthormi, Maurer et al., 2016). These changes are consistent with the accelerating mass loss of glaciers in northern Bhutan. The regional mass balances in northern Bhutan have accelerated from the 1974–2006 period to the post 2000 period. For example, the region-wide mass balance is  $-0.17 \pm 0.05 \text{ m w.e. a}^{-1}$  for 1974–2006 (Maurer et al., 2016),  $-0.22 \pm 0.12 \text{ m w.e. a}^{-1}$  for 1999–2011 (Gardelle et al., 2013),  $-0.42 \pm 0.20 \text{ m w.e. a}^{-1}$  for 2000–2016 (Brun et al., 2017) and  $-0.52 \pm 0.16 \text{ m w.e. a}^{-1}$  for 2003–2008 (Kääb et al., 2012). The mass change of Bhutanese glaciers is expected to be sensitive to precipitation, which varies under the influence of the summer monsoon (Fujita and Ageta, 2000; Fujita, 2008). The summer monsoon has been weakening since the 1950s (Bollasina et al., 2011), which might have reduced the amount of snowfall across the present study area. This trend is likely one of the reasons for the accelerated glacier thinning in recent years. However, care should be taken in making such inferences because previous studies covered different spatial extents, used different methods to fill data gaps in the accumulation areas, and suffered from uncertainties in SRTM data due to radar penetration (Zemp et al., 2015; Maurer et al., 2016). Regardless, the thinning rate increased by a greater amount at Lugge Glacier than at Thorthormi Glacier from 1974–2006 to 2004–2011, indicating that the rapid thinning of Lugge Glacier is affected by a change in ice dynamics. A likely interpretation is that the expansion of Lugge Glacial Lake after the 1960s and glacier thinning decreased the effective pressure (ice overburden minus basal water pressure), resulting in glacier acceleration by enhancing basal ice motion, as previously seen near the front of a lake-terminating glacier (Sugiyama et al., 2011). It is likely that the acceleration and enhanced longitudinal stretching near the terminus resulted in further ice thinning.

## 5.2 Influence of ice dynamics on glacier thinning

The simulated SMB of Lugge Glacier for the 1979–2017 period ( $-6.77 \pm 0.17 \text{ m w.e. a}^{-1}$ ) is 1.6 times more negative than its thinning rate for the 2004–2011 period ( $-4.25 \pm 0.02 \text{ m w.e. a}^{-1}$ ), which is converted to water equivalent using an ice density of  $910 \text{ kg m}^{-3}$ , while the negative SMB of Thorthormi Glacier ( $-9.03 \pm 0.14 \text{ m w.e. a}^{-1}$ ) is 7.1 times more negative than its thinning rate ( $-1.27 \pm 0.01 \text{ m w.e. a}^{-1}$ ). This result suggests that the rapid thinning is due mainly to surface melting along Lugge Glacier, whereas the negative SMB is counterbalanced by the vertical straining of Thorthormi Glacier (Figs. 6c and 6d).

The horizontal flow velocities of Lugge Glacier are nearly uniform along the central flowline, with ice flow parallel to the glacier surface (Fig. 6d), suggesting that the dynamically induced change in ice thickness is small. However, the flow velocities of Thorthormi Glacier decrease toward the terminus (Fig. 6c), resulting in thickening under a longitudinally compressive flow regime. The computed emergence velocity of Lugge Glacier is slightly negative ( $-0.2 \pm 0.1$  m w.e.  $a^{-1}$ ), suggesting that the contribution of dynamic ice thickness change to ice thinning is small, with the significant thinning of Lugge Glacier caused mainly by its negative SMB. However, the emergence velocity of Thorthormi Glacier is positive ( $3.1 \pm 0.4$  m w.e.  $a^{-1}$ ), suggesting that the glacier is thickening due to a vertically straining flow regime. The mean SMB of Thorthormi Glacier is 33 % more negative than that of Lugge Glacier. Since a sparse distribution of thin debris cover is present across the ablation area of both glaciers, the more negative SMB of Thorthormi Glacier cannot be fully explained by differences in the thickness and spatial distribution of debris cover, with a more likely explanation being that the glacier is situated at lower elevations (Figs. 6a and 6b). The calculated rate of elevation change over the surveyed domain of Thorthormi Glacier is equivalent to one-fourth of the SMB, implying that approximately three-fourths of the surface ablation is counterbalanced by ice dynamics. In other words, dynamically induced thickening compensates for the negative SMB.

Experiment 1 demonstrates that the difference in emergence velocity between land- and lake-terminating glaciers leads to contrasting thinning patterns. Based on this result, we hypothesise that the emergence velocity of Lugge Glacier would be positive in the absence of a glacial lake. Furthermore, the emergence velocity of Thorthormi Glacier will decrease in association with lake development. The results from Experiments 1 and 2 support this hypothesis, with a positive emergence velocity ( $1.4 \pm 0.1$  m w.e.  $a^{-1}$ ) modelled for Lugge Glacier under the land-terminating condition, resulting in a decrease in the thinning rate of 28 % compared with the lake-terminating condition. This result suggests that the decrease in emergence velocity caused by the development of Lugge Glacial Lake should have accelerated the thinning in addition to the more negative SMB since the 1960s. For Thorthormi Glacier, the emergence velocity under the lake-terminating condition is still positive ( $1.8 \pm 0.4$  m w.e.  $a^{-1}$ ) but it decreases by 72 % from the land-terminating condition, resulting in an increase in the thinning rate from 6.1 to 7.4 m  $a^{-1}$ . Our ice flow modelling demonstrates that thinning will accelerate in association with the development of a supraglacial lake in the terminal part of Thorthormi Glacier.

Contrasting patterns of glacier thinning and horizontal flow velocities between land- and lake-terminating glaciers are consistent with satellite-based observations over lake or ocean-terminating glaciers and neighbouring land-terminating glaciers in the Nepal Himalaya (King et al., 2017) and Greenland (Tsutaki et al., 2016). A decrease in the down-glacier flow velocities over the lower reaches of land-terminating glaciers suggests a longitudinally compressive flow regime, which would result in a positive emergence velocity and therefore less thinning to compensate for the negative SMB, as demonstrated in the ice flow model. Conversely, for lake-terminating glaciers, an increase in the down-glacier flow velocities suggests a longitudinally stretching flow regime, which would yield a negative emergence velocity, resulting in accelerated ice thinning. Such mechanisms should not only be active for Thorthormi and Lugge glaciers, but any lake- and land-terminating glaciers worldwide where contrasting thinning patterns between glaciers are observed.

520 The thinning rate calculated from the model is  $\sim 5 \text{ m a}^{-1}$  more negative than the observation over the entire domain of Lugge  
Glacier and also the lower part of Thorthormi Glacier (Fig. 8b), which is probably due to the uncertainties in the estimated ice  
thickness and basal sliding conditions as discussed in section 4.5.3. The two-dimensional feature is another reason for the  
insufficient modelled results because the model neglects drag from the side walls and changes in glacier width. The SMB  
(meltwater) uncertainty is  $< 50 \%$  over a large portion of Thorthormi and Lugge glaciers (Fig. S10). Nevertheless, our  
525 numerical experiments demonstrate that dynamically induced ice thickening compensates the negative SMB in the lower part  
of a land-terminating glacier, resulting in less ice thinning in comparison with a lake-terminating glacier. Further measurements  
of the spatial distributions of ice thickness and SMB will help in deriving more accurate estimates of the effect of ice dynamics  
on glacier thinning.

### 5.3 Glacier retreat

530 Lugge Glacier has retreated continuously and at a nearly constant rate from 2000 to 2011 (Fig. 5). The mean rate of area change  
over the 2000–2010 period ( $-0.03 \text{ km}^2 \text{ a}^{-1}$ ) is comparable to a previously reported value for 2000–2010 ( $-0.04 \text{ km}^2 \text{ a}^{-1}$ ,  
Bajracharya et al., 2014). Bathymetric data suggest that glacier ice below the lake level accounted for 89 % of the full ice  
thickness at the calving front in 2002 (Fig. 6b). The lake level is close to the ice flotation level, where the basal water pressure  
equals the ice overburden pressure, suggesting that calving caused by ice flotation regulates the glacier front position (van der  
535 Veen, 1996). Glaciers rapidly retreat by calving when the lake level reaches the flotation level (e.g., Motyka et al., 2002;  
Tsutaki et al., 2011). Moreover, retreat is accelerated when the glacier terminus is situated on a reversed bed slope (e.g., Nick  
et al., 2009). A recent numerical study estimated overdeepening of Lugge Glacier within 1500 m of the 2009 terminus  
(Linsbauer et al., 2016), suggesting further rapid retreat in the future. Recent glacier inventories indicate that Lugge Glacier  
has a smaller accumulation area than Thorthormi Glacier (Nuimura et al., 2015; Nagai et al., 2016), suggesting that a sufficient  
540 ice flux cannot be supplied to the lower part of the glacier to compensate for the ongoing ice thinning.

The mean rate of area change for Thorthormi Glacier over the 2000–2010 period ( $-0.09 \text{ km}^2 \text{ a}^{-1}$ ) is comparable to a  
previously reported value for 2000–2010 ( $-0.04 \text{ km}^2 \text{ a}^{-1}$ , Bajracharya et al., 2014). After progressive mass loss since 2000, the  
front of Thorthormi Glacier detached from the terminal moraine and retreated further from November 2010 to December 2011  
(Fig. 4a). The glacier ice was still in contact with the moraine during the field campaign in September 2011, but the glacier  
545 was completely detached from the moraine on the 2 December 2011 Landsat 7 image. Satellite images taken after 2 December  
2011 show a large number of icebergs floating in the lake, suggesting rapid calving due to ice flotation. A numerical study  
suggested that a proglacial lake longer than a certain longitudinal length is also preferable for autonomous expansion through  
valley wind over the lake surface (Sakai et al., 2009). A previous study estimated that the overdeepening of Thorthormi Glacier  
extends for  $> 3000 \text{ m}$  from the terminal moraine (Linsbauer et al., 2016), which suggests that continued glacier thinning will  
550 lead to rapid retreat of the entire section of the terminus as the ice thickness reaches flotation.

Experiment 2 simulates a significant increase in surface flow velocity at the lower part of Thorthormi Glacier when a proglacial lake forms (Fig. 7e). Previous studies reported the speed up and rapid retreat of glaciers after detachment from a terminal ridge or bedrock bump (e.g., Boyce et al., 2007; Sakakibara and Sugiyama, 2014; Trüssel et al., 2015). In addition to the reduction in back stress, thinning itself decreases the effective pressure, which enhances basal ice motion and increases the flow velocity (Sugiyama et al., 2011). A decrease in the effective pressure also enhances shear stress in the water saturated till layer beneath the glacier (Cuffey and Paterson, 2010), though little information is available on subglacial sedimentation in the Himalayas. Acceleration near the terminus results in ice thinning and a decrease in effective pressure, which in turn leads to further acceleration of glacier flow (e.g., Benn et al., 2007b). Although no clear acceleration was observed during 2002–2011 (Fig. 3a), it is likely that the thinning and retreat of Thorthormi Glacier will be accelerated in the near future due to the formation and expansion of the proglacial lake.

## 6 Conclusions

To better understand the importance of glacial lake formation on rapid glacier thinning, we carried out field and satellite-based measurements across the lake-terminating Lugge Glacier and the land-terminating Thorthormi Glacier in the Lunana region, Bhutan Himalaya. Surface elevations were surveyed in 2011 by differential GPS across the lower parts of the glaciers and compared with a 2004 GPS survey. The flow velocity and terminus positions of the glaciers were determined from optical satellite images. We also performed numerical experiments to quantify the contributions of surface mass balance (SMB) and ice dynamics in relation to the observed ice thinning.

Lugge Glacier has experienced rapid ice thinning at an average rate of  $-4.67 \pm 0.02 \text{ m a}^{-1}$ , which is 3.3 times greater than that of Thorthormi Glacier, even though the SMB was less negative. The numerical modelling results, using the present glacier geometries, demonstrate that Thorthormi Glacier is subjected to a longitudinally compressive flow regime, suggesting that dynamically induced thickening compensates for the negative SMB, and thus results in less ice thinning than at Lugge Glacier. Conversely, the flow of Lugge Glacier is nearly uniform along its central flowline, suggesting that the dynamically induced change in ice thickness is small, with the rapid thinning of Lugge Glacier driven by surface melt. This study reveals that contrasting ice flow regimes cause different ice thinning observations between lake- and land-terminating glaciers in the Bhutan Himalaya.

Lugge Glacier retreated continuously from 2000 to 2011, shrinking at a rate of  $0.03 \text{ km}^2 \text{ a}^{-1}$ . The ice approaching the calving front is near flotation, suggesting that the terminus retreat will be accelerated by active calving in the future. Thorthormi Glacier has been retreating since 2000, resulting in the detachment of the glacier front from the terminal moraine and the formation of a proglacial lake in 2011. Ice flow modelling with the lake-terminating boundary condition indicates a significant increase in surface flow velocities near the calving front, which leads to continued glacier retreat. This positive feedback will

be activated in Thorthormi Glacier with the expansion of the proglacial lake, causing further thinning and retreat in the near future.

**Data availability.** The data for Figs. 1–8 are provided in Microsoft Excel format in the Supplement. The ALOS satellite data are available for purchase from the Remote Sensing Technology Center of Japan (<https://www.restec.or.jp/en/>). The Landsat 7 ETM+ satellite data are distributed by the United States Geological Survey (<http://landsat.usgs.gov/>).

**Author contributions.** KF and AS designed the study. KF, JK, TN, PT, and ST conducted the field survey in 2011. KF analysed the survey data in 2004 and 2011, and simulated the surface mass balance. TN calculated the satellite-based surface flow velocities. SS provided ice flow models. ST analysed the data. ST and KF wrote the paper, with contributions from AS and SS.

**Competing interests.** The authors declare that they have no conflict of interest.

**Acknowledgement.** We thank the Department of Geology and Mines, Bhutan, for providing the opportunity and permission to conduct the field observations. We thank S. Takenaka, M. Sano, A. Sasaki, K. Ghallay and logistic members for their support during the field campaign. We appreciate F. Pellicciotti and three anonymous referees for their thoughtful and constructive comments. This research was supported by the Science and Technology Research Partnership for Sustainable Development (SATREPS), supported by the Japan Science and Technology Agency (JST) and the Japan International Cooperation Agency (JICA). Support was also provided by the Funding Program for Next Generation World Leading Researchers (NEXT Program, GR052), and JSPS-KAKENHI (grant numbers 26257202 and 17H06104).

## References

- Ageta, Y., Iwata, S., Yabuki, H., Naito, N., Sakai, A., Narama, C., and Karma.: Expansion of glacier lakes in recent decades in the Bhutan Himalayas, *IAHS Publ.*, 264, 165–175, 2000.
- Azam, M. F., Wagnon, P., Berthier, E., Vincent, C., Fujita, K., and Kargel, J. S.: Review of the status and mass changes of Himalayan-Karakoram glaciers, *J. Glaciol.*, 1–14, <https://doi.org/10.1017/jog.2017.86>, 2018.
- Bajracharya, S. R., Maharjan, S. B., and Shrestha, F.: The status and decadal change of glaciers in Bhutan from the 1980s to 2010 based on satellite data, *Ann. Glaciol.*, 55 (66), 159–166, <https://doi.org/10.3189/2014AoG66A125>, 2014.
- Benn D., Hulton, N. R. J., and Mottram, R. H.: ‘Calving lows’, ‘sliding laws’, and the stability of tidewater glaciers, *Ann. Glaciol.*, 46 (1), 123–130, <https://doi.org/10.3189/172756407782871161>, 2007a.

- Benn, D., Warren, C., and Mottram, R.: Calving processes and the dynamics of calving glaciers, *Earth-Sci. Rev.*, 82, 143–179, <https://doi.org/10.1016/j.earscirev.2007.02.002>, 2007b.
- Berthier, E., Arnaud, Y., Kumar, R., Ahmad, S., Wagnon, P., and Chevallier, P.: Remote sensing estimates of glacier mass balances in the Himachal Pradesh (Western Himalaya, India), *Remote Sens. Environ.*, 108 (3), 327–338, 615 <https://doi.org/10.1016/j.rse.2006.11.017>, 2007.
- Bolch, T., Pieczonka, T., and Benn, D. I.: Multi-decadal mass loss of glaciers in the Everest area (Nepal Himalaya) derived from stereo imagery, *The Cryosphere*, 5 (2), 349–358, <https://doi.org/10.5194/tc-5-349-2011>, 2011.
- Bolch, T., Kulkarni, A., Kääb, A., Huggel, C., Paul, F., Cogley, J. G., Frey, H., Kargel, J. S., Fujita, K., Scheel, M., Bajracharya, S., Stoffel, M.: The state and fate of Himalayan Glaciers, *Science*, 336 (6079), 310–314, 620 <https://doi.org/10.1126/science.1215828>, 2012.
- Bollasina, M., Ming, Y., and Ramaswamy, V.: Anthropogenic aerosols and the weakening of the South Asian summer monsoon, *Science*, 334, 502–505, <https://doi.org/10.1126/science.1204994>, 2011.
- Boyce, E. S., Motyka, R. J., and Truffer, M.: Flotation and retreat of a lake-calving terminus, Mendenhall Glacier, southeast Alaska, USA, *J. Glaciol.*, 53 (181), 211–224, <https://doi.org/10.3189/172756507782202928>, 2007.
- 625 Brun, F., Berthier, E., Wagnon, P., Kääb, A., and Treichler, D.: A spatially resolved estimate of High Mountain Asia glacier mass balances from 2000 to 2016, *Nat. Geosci.*, 10, 668–673, <https://doi.org/10.1038/ngeo2999>, 2017.
- Carrivick, J. L., and Tweed, F. S.: Proglacial lakes: character, behaviour and geological importance, *Quaternary Sci. Rev.*, 78, 34–52, <https://doi.org/10.1016/j.quascirev.2013.07.028>, 2013.
- Cogley, J. G.: Glacier shrinkage across High Mountain Asia, *Ann. Glaciol.*, 57 (71), 41–49, 630 <https://doi.org/10.3189/2016AoG71A040>, 2016.
- Cuffey, K. M. and Paterson, W. S. B.: *The physics of glaciers*, Oxford, Butterworth-Heinemann, 2010.
- Dehecq, A., Gourmelen, N., and Trouve, E.: Deriving large-scale glacier velocities from a complete satellite archive: Application to the Pamir–Karakoram–Himalaya, *Remote Sens. Environ.*, 162, 55–66, <https://doi.org/10.1016/j.rse.2015.01.031>, 2015.
- 635 Farinotti, D., Huss, M., Bauder, A., Funk, M., and Truffer, M.: A method to estimate the ice volume and ice-thickness distribution of alpine glaciers, *J. Glaciol.*, 55 (191), 422–430, <https://doi.org/10.3189/002214309788816759>, 2009.
- Fujita, K.: Effect of precipitation seasonality on climatic sensitivity of glacier mass balance, *Earth Planet. Sci. Lett.*, 276 (1–2), 14–19, <https://doi.org/10.1016/j.epsl.2008.08.028>, 2008.
- Fujita, K., and Ageta, Y.: Effect of summer accumulation on glacier mass balance on the Tibetan Plateau revealed by mass- 640 balance model, *J. Glaciol.*, 46 (153), 244–252, <https://doi.org/10.3189/172756500781832945>, 2000.
- Fujita, K., and Nuimura, T.: Spatially heterogeneous wastage of Himalayan glaciers, *P. Natl. Acad. Sci. USA*, 108 (34), 14011–14014, <https://doi.org/10.1073/pnas.1106242108>, 2011.

- Fujita, K., and Sakai, A.: Modelling runoff from a Himalayan debris-covered glacier, *Hydrol. Earth Syst. Sci.*, 18 (7), 2679–2694, <https://doi.org/10.5194/hess-18-2679-2014>, 2014.
- 645 Fujita, K., Suzuki, R., Nuimura, T., and Sakai, A.: Performance of ASTER and SRTM DEMs, and their potential for assessing glacial lakes in the Lunana region, Bhutan Himalaya, *J. Glaciol.*, 54 (185), 220–228, <https://doi.org/10.3189/002214308784886162>, 2008.
- Fujita, K., Sakai, A., Nuimura, T., Yamaguchi, S., and Sharma, R. R.: Recent changes in Imja Glacial Lake and its damming moraine in the Nepal Himalaya revealed by in situ surveys and multi-temporal ASTER imagery, *Environ. Res. Lett.*, 4 (4), 650 045205, <https://doi.org/10.1088/1748-9326/4/4/045205>, 2009.
- Fujita, K., Takeuchi, N., Nikitin, S. A., Surazakov, A. B., Okamoto, S., Aizen, V. B., and Kubota, J.: Favorable climatic regime for maintaining the present-day geometry of the Gregoriev Glacier, Inner Tien Shan, *The Cryosphere*, 5 (3), 539–549, <https://doi.org/10.5194/tc-5-539-2011>, 2011.
- Fujita, K., Sakai, A., Takenaka, S., Nuimura, T., Surazakov, A. B., Sawagaki, T., and Yamanokuchi, T.: Potential flood volume 655 of Himalayan glacial lakes, *Nat. Hazards Earth Syst. Sci.*, 13 (7), 1827–1839, <https://doi.org/10.5194/nhess-13-1827-2013>, 2013.
- Funk, M., and Röthlisberger, H.: Forecasting the effects of a planned reservoir which will partially flood the tongue of Unteraargletscher in Switzerland, *Ann. Glaciol.*, 13, 76–81, <https://doi.org/10.1017/S0260305500007679>, 1989.
- Gardelle, J., Arnaud, Y., and Berthier, E.: Contrasted evolution of glacial lakes along the Hindu Kush Himalaya mountain 660 range between 1990 and 2009, *Global Planet. Change*, 75 (1–2), 47–55, <https://doi.org/10.1016/j.gloplacha.2010.10.003>, 2011.
- Gardelle, J., Berthier, E., Arnaud, Y., and Käab, A.: Region-wide glacier mass balances over the Pamir-Karakoram-Himalaya during 1999–2011, *The Cryosphere*, 7 (4), 1263–1286, <https://doi.org/10.5194/tc-7-1263-2013>, 2013.
- Glen, J. W.: The creep of polycrystalline ice, *Proc. R. Soc. London, Sea. A*, 228 (1175), 519–538, 665 <https://doi.org/10.1098/rspa.1955.0066>, 1955.
- Gudmundsson, G. H.: A three-dimensional numerical model of the confluence area of Unteraargletscher, Bernese Alps, Switzerland, *J. Glaciol.*, 45 (150), 219–230, <https://doi.org/10.3198/1999JoG45-150-219-230>, 1999.
- Heid, T., and Käab, A.: Evaluation of existing image matching methods for deriving glacier surface displacements globally from optical satellite imagery, *Remote Sens. Environ.*, 118, 339–355, <https://doi.org/10.1016/j.rse.2011.11.024>, 2012.
- 670 Hewitt, H. and Liu, J.: Ice-dammed lakes and outburst floods, Karakoram Himalaya: historical perspectives on emerging threats, *Physical Geography*, 31 (6), 528–551, <https://doi.org/10.2747/0272-3646.31.6.528>, 2010.
- Huss, M., and Hock, R.: Global-scale hydrological response to future glacier mass loss, *Nature Climate Change*, 8, 135–140, <https://doi.org/10.1038/s41558-017-0049-x>, 2018.
- Immerzeel, W. W., Van Beek, L. P., and Bierkens, M. F.: Climate change will affect the Asian water towers, *Science*, 328 675 (5984), 1382–1385, <https://doi.org/10.1126/science.1183188>, 2010.

- Kääb, A.: Combination of SRTM3 and repeat ASTER data for deriving alpine glacier flow velocities in the Bhutan Himalaya, *Remote Sens. Environ.*, 94, 463–474, <https://doi.org/10.1016/j.rse.2004.11.003>, 2005.
- Kääb, A., Berthier, E., Nuth, C., Gardelle, J., and Arnaud, Y.: Contrasting patterns of early twenty-first-century glacier mass change in the Himalayas, *Nature*, 488 (7412), 495–498, <https://doi.org/10.1038/nature11324>, 2012.
- 680 Kanamitsu, M., Ebisuzaki, W., Woollen, J., Yang, S-K., Hnilo, J. J., Fiorino, M., and Potter., G. L.: NCEP-DOE AMIP-II Reanalysis (R-2), *B. Am. Meteorol. Soc.*, 1631–1643, <https://doi.org/10.1175/BAMS-83-11-1631>, 2002.
- King, O., Quincey, D. J., Carrivick, J. L., and Rowan, A. V.: Spatial variability in mass loss of glaciers in the Everest region, central Himalayas, between 2000 and 2015, *The Cryosphere*, 11 (1), 407–426, <https://doi.org/10.5194/tc-11-407-2017>, 2017.
- Komori, J.: Recent expansions of glacial lakes in the Bhutan Himalayas, *Quatern. Int.*, 184 (1), 177–186, <https://doi.org/10.1016/j.quaint.2007.09.012>, 2008.
- 685 Lamsal, D., Fujita, K., and Sakai, A.: Surface lowering of the debris-covered area of Kanchenjunga Glacier in the eastern Nepal Himalaya since 1975, as revealed by Hexagon KH-9 and ALOS satellite observations, *The Cryosphere*, 11, 2815–2827, <https://doi.org/10.5194/tc-11-2815-2017>, 2017.
- Leprince, S., Barbot, S., Ayoub, F., and Avouac, J-P.: Automatic and precise orthorectification, coregistration, and subpixel correlation of satellite images, application to ground deformation measurements, *IEEE Trans. Geosci. Remote Sens.*, 45, 1529–1558, <https://doi.org/10.1109/TGRS.2006.888937>, 2007.
- 690 Linsbauer, A., Frey, H., Haerberli, W., Machguth, H., Azam, M., and Allen, S.: Modelling glacier-bed overdeepenings and possible future lakes for the glaciers in the Himalaya–Karakoram region, *Ann. Glaciol.*, 57 (71), 119–130, <https://doi.org/10.3189/2016AoG71A627>, 2016.
- 695 Mattson, L. E., Gardner, J. S., and Young, G. J.: Ablation on debris covered glaciers: an example from the Rakhiot Glacier, Punjab, Himalaya, *IAHS Publication*, 218, 289–296, 1993.
- Maurer, J. M., Rupper, S. B., and Schaefer, J. M.: Quantifying ice loss in the eastern Himalayas since 1974 using declassified spy satellite imagery, *The Cryosphere*, 10 (5), 2203–2215, doi:10.5194/tc-10-2203-2016, 2016.
- Mölg, T., Maussion, F., and Scherer, D.: Mid-latitude westerlies as a driver of glacier variability in monsoonal High Asia, *Nature Climate Change*, 4, 68–73, <https://doi.org/10.1038/nclimate2055>, 2014.
- 700 Motyka, R. J., O’Neel, S., Connor, C. L., and Echelmeyer, K. A.: Twentieth century thinning of Mendenhall Glacier, Alaska, and its relationship to climate, lake calving, and glacier runoff, *Global Planet. Change*, 35 (1–2), 93–112, [https://doi.org/10.1016/S0921-8181\(02\)00138-8](https://doi.org/10.1016/S0921-8181(02)00138-8), 2002.
- Nagai, H., Fujita, K., Sakai, A., Nuimura, T., and Tadono, T.: Comparison of multiple glacier inventories with a new inventory derived from high-resolution ALOS imagery in the Bhutan Himalaya, *The Cryosphere*, 10 (1), 65–85, <https://doi.org/10.5194/tc-10-65-2016>, 2016.
- 705 Naito, N., Suzuki, R., Komori, J., Matsuda, Y., Yamaguchi, S., Sawagaki, T., and Tshering, P.: Recent glacier shrinkages in the Lunana region, Bhutan Himalayas, *Global Environ. Res.*, 16 (1), 13–22, 2012.

- 710 Nick, F. M., Vieli, A., Howat, I. M., and Joughin, I.: Large-scale changes in Greenland outlet glacier dynamics triggered at the terminus, *Nature Geosci.*, 2 (2), 110–114, <https://doi.org/10.1038/ngeo394>, 2009.
- Nie, Y., Sheng, Y., Liu, Q., Liu, L., Liu, S., Zhang, Y., and Song, C.: A regional-scale assessment of Himalayan glacial lake changes using satellite observations from 1990 to 2015, *Remote Sens. Environ.*, 189, 1–13, <https://doi.org/10.1016/j.rse.2016.11.008>, 2017.
- 715 Nuimura, T., Fujita, K., Yamaguchi, S., and Sharma, R. R.: Elevation changes of glaciers revealed by multitemporal digital elevation models calibrated by GPS survey in the Khumbu region, Nepal Himalaya, 1992–2008, *J. Glaciol.*, 58 (210), 648–656, <https://doi.org/10.3189/2012JoG11J061>, 2012.
- Nuimura, T., Sakai, A., Taniguchi, K., Nagai, H., Lamsal, D., Tsutaki, S., Kozawa, A., Hoshina, Y., Takenaka, S., Omiya, S., Tsunematsu, K., Tshering, P., and Fujita, K.: The GAMDAM glacier inventory: a quality-controlled inventory of Asian glaciers, *The Cryosphere*, 9 (3), 849–864, <https://doi.org/10.5194/tc-9-849-2015>, 2015.
- 720 Østrem, G.: Ice melting under a thin layer of moraine and the existence of ice cores in moraine ridges, *Geogr. Ann.*, 41, 228–230, 1959.
- Paul, F., Barrand, N. E., Berthier, E., Bolch, T., Casey, K., Frey, H., Joshi, S. P., Kononov, V., Le Bris, R., Mölg, N., Nuth, C., Pope, A., Racoviteanu, A., Rastner, P., Raup, B., Scharrer, K., Steffen, S., and Winswold, S.: On the accuracy of glacier outlines derived from remote sensing data, *Ann. Glaciol.*, 54 (63), 171–182, <https://doi.org/10.3189/2013AoG63A296>, 2013.
- 725 Reid, T. D. and Brock, B. W.: An energy-balance model for debris-covered glaciers including heat conduction through the debris layer, *J. Glaciol.*, 56 (199), 903–916, <https://doi.org/10.3189/002214310794457218>, 2010.
- Sakai, A.: Glacial Lakes in the Himalayas: A Review on Formation and Expansion Processes, *Global Environ. Res.*, 16 (1), 23–30, 2012.
- Sakai, A. and Fujita, K.: Formation conditions of supraglacial lakes on debris-covered glaciers in the Himalayas, *J. Glaciol.*, 56 (195), 177–181, <https://doi.org/10.3189/002214310791190785>, 2010.
- 730 Sakai, A. and Fujita, K.: Contrasting glacier responses to recent climate change in high-mountain Asia, *Sci. Rep.*, 7 (1), 13717, <https://doi.org/10.1038/s41598-017-14256-5>, 2017.
- Sakai, A., Nishimura, K., Kadota, T., and Takeuchi, N.: Onset of calving at supraglacial lakes on debris covered glaciers of the Nepal Himalayas, *J. Glaciol.*, 55 (193), 909–917, <https://doi.org/10.3189/002214309790152555>, 2009.
- 735 Sakai, A., Nuimura, T., Fujita, K., Takenaka, S., Nagai, H., and Lamsal, D.: Climate regime of Asian glaciers revealed by GAMDAM glacier inventory, *The Cryosphere*, 9, 865–880, <https://doi.org/10.5194/tc-9-865-2015>, 2015.
- Sakakibara, D. and Sugiyama, S.: Ice-front variations and speed changes of calving glaciers in the Southern Patagonia Icefield from 1984 to 2011, *J. Geophys. Res.-Earth*, 119, 2541–2554, <https://doi.org/10.1002/2014JF003148>, 2014.
- 740 Scherler, D., and Strecker, M. R.: Large surface velocity fluctuations of Biafo Glacier, central Karakoram, at high spatial and temporal resolution from optical satellite images, *J. Glaciol.*, 58 (209), 569–580, <https://doi.org/10.3189/2012JoG11J096>, 2012.

- Scherler, D., Bookhagen, B., and Strecker, M. R.: Spatially variable response of Himalayan glaciers to climate change affected by debris cover, *Nat. Geosci.*, 4 (3), 156–159, <https://doi.org/10.1038/ngeo1068>, 2011a.
- 745 Scherler, D., Bookhagen, B., and Strecker, M. R.: Hillslope glacier coupling: The interplay of topography and glacial dynamics in High Asia, *J. Geophys. Res.*, 116, F02019, <https://doi.org/10.1029/2010JF001751>, 2011b.
- Sugiyama, S., Gudmundsson, G. H., and Helbing, J.: Numerical investigation of the effects of temporal variations in basal lubrication on englacial strain-rate distribution, *Ann. Glaciol.*, 37, 49–54, <https://doi.org/10.3189/172765403781815618>, 2003.
- 750 Sugiyama, S., Skvarca, P., Naito, N., Enomoto, H., Tsutaki, S., Tone, K., Marinsek, S., and Aniya, M.: Ice speed of a calving glacier modulated by small fluctuations in basal water pressure, *Nat. Geosci.*, 4 (9), 597–600, <https://doi.org/10.1038/ngeo1218>, 2011.
- Sugiyama, S., Sakakibara, D., Matsuno, S., Yamaguchi, S., Matoba, S., Aoki, T.: Initial field observation on Qaanaaq ice cap, northwestern Greenland, *Ann. Glaciol.*, 55 (66), 25–33, <https://doi.org/10.3189/2014AoG66A102>, 2014.
- 755 Suzuki, R., Fujita, K., and Ageta, Y.: Spatial distribution of thermal properties on debris-covered glaciers in the Himalayas derived from ASTER data, *Bull. Glaciol. Res.*, 24, 13–22, 2007a.
- Suzuki, R., Fujita, K., Ageta, Y., Naito, N., Matsuda, Y., and Karma: Meteorological observations during 2002–2004 in Lunana region, Bhutan Himalayas, *Bull. Glaciol. Res.*, 24, 71–78, 2007b.
- Truffer, M., Motyka, R. J., Hekkers, M., Howat, I. M., and King, M. A.: Terminus dynamics at an advancing glacier: Taku Glacier, Alaska, *J. Glaciol.*, 55 (194), 1052–1060, <https://doi.org/10.3189/002214309790794887>, 2009.
- 760 Trüssel, B. L., Motyka, R. J., Truffer, M., and Larsen, C. F.: Rapid thinning of lake-calving Yakutat Glacier and the collapse of the Yakutat Icefield, southeast Alaska, USA, *J. Glaciol.*, 59 (215), 149–161, <https://doi.org/10.3189/2013JoG12J081>, 2013.
- Trüssel, B. L., Truffer, M., Hock, R., Motyka, R. J., Huss, M., and Zhang, J.: Runaway thinning of the low-elevation Yakutat Glacier, Alaska, and its sensitivity to climate change, *J. Glaciol.*, 61 (225), 65–75, <https://doi.org/10.3189/2015JoG14J125>, 765 2015.
- Tshering, P., and Fujita, K.: First in situ record of decadal glacier mass balance (2003–2014) from the Bhutan Himalaya, *Ann. Glaciol.*, 57 (71), 289–294, <https://doi.org/10.3189/2016AoG71A036>, 2016.
- Tsutaki, S., Nishimura, D., Yoshizawa, T., and Sugiyama, S.: Changes in glacier dynamics under the influence of proglacial lake formation in Rhonegletscher, Switzerland, *Ann. Glaciol.*, 52 (58), 31–36, 770 <https://doi.org/10.3189/172756411797252194>, 2011.
- Tsutaki, S., Sugiyama, S., Nishimura, D., and Funk, M.: Acceleration and flotation of a glacier terminus during formation of a proglacial lake in Rhonegletscher, Switzerland, *J. Glaciol.*, 59 (215), 559–570, <https://doi.org/10.3189/2013JoG12J107>, 2013.

- Tsutaki, S., Sugiyama, S., Sakakibara, D., and Sawagaki, T.: Surface elevation changes during 2007–13 on Bowdoin and Tugto  
775      Glaciers, northwestern Greenland, *J. Glaciol.*, 62 (236), 1083–1092, <https://doi.org/10.1017/jog.2016.106>, 2016.
- van der Veen, C. J.: Tidewater calving, *J. Glaciol.*, 42 (141), 375–385, doi:10.1017/S0022143000004226, 1996.
- Vieli, A., and Nick, F. M.: Understanding and modelling rapid dynamic changes of tidewater outlet glaciers: issues and  
implications, *Surv. Geophys.*, 32, 437–458, <https://doi.org/10.1007/s10712-011-9132-4>, 2011.
- Vincent, C., Wagnon, P., Shea, J. M., Immerzeel, W. W., Kraaijenbrink, P., Shrestha, D., Soruco, A., Arnaud, Y., Brun, F.,  
780      Berthier, E., and Sherpa, S. F.: Reduced melt on debris-covered glaciers: investigations from Changri Nup Glacier, Nepal,  
*The Cryosphere*, 10 (4), 1845–1858, <https://doi.org/10.5194/tc-10-1845-2016>, 2016.
- Warren, C. R., and Kirkbride, M. P.: Calving speed and climatic sensitivity of New Zealand lake-calving glaciers, *Ann. Glaciol.*,  
36, 173–178, <https://doi.org/10.3189/172756403781816446>, 2003.
- Yamada, T., Naito, N., Kohshima, S., Fushimi, H., Nakazawa, F., Segawa, T., Uetake, J., Suzuki, R., Sato, N., Karma, Chhetri,  
785      I. K., Gyenden, L., Yabuki, H., and Chikita, K.: Outline of 2002 – research activities on glaciers and glacier lakes in Lunana  
region, Bhutan Himalaya, *Bull. Glaciol. Res.*, 21, 79–90, 2004.
- Yao, T., Thompson, L., Yang, W., Yu, W., Gao, Y., Guo, X., Yang, X., Duan, K., Zhao, H., Xu, B., Pu, J., Lu, A., Xiang, Y.,  
Kattel, D. B., and Joswiak, D.: Different glacier status with atmospheric circulations in Tibetan Plateau and surroundings,  
*Nature Climate Change*, 2, 663–667, <https://doi.org/10.1038/nclimate1580>, 2012.
- 790      Zhang, Y., Fujita, K., Liu, S. Y., Liu, Q., and Nuimura, T.: Distribution of debris thickness and its effect on ice melt at  
Hailuoguo glacier, southeastern Tibetan Plateau, using in situ surveys and ASTER imagery, *J. Glaciol.*, 57 (206), 1147–  
1157, <https://doi.org/10.3189/002214311798843331>, 2011.
- Zemp, M., Frey, H., Gärtner-Roer, I., Nussbaumer, S. U., Hoelzle, M., Paul, F., Haeberli, W., Denzinger, F., Ahlstrøm, A. P.,  
Anderson, B., Bajracharya, S., Baroni, C., Braun, L. N., Cáceres, B. E., Casassa, G., Cobos, G., Dávila, L. R., Delgado  
795      Granados, H., Demuth, M. N., Espizua, L., Fischer, A., Fujita, K., Gadek, B., Ghazanfar, A., Hagen, J. O., Holmlund, P.,  
Karimi, N., Li, Z. Q., Pelto, M., Pitte, P., Popovnin, V. V., Portocarrero, C. A., Prinz, R., Sangewar, C. V., Severskiy, I.,  
Sigurðsson, O., Soruco, A., Usubaliev, R., and Vincent, C.: Historically unprecedented global glacier decline in the early  
21st century, *J. Glaciol.*, 61 (228), 745–761, <https://doi.org/10.3189/2015JoG15J017>, 2015.

800

805

810

815

820

**Table 1:** Observed elevation changes ( $dh$ ) and rate of elevation changes ( $dh/dt$ ), with standard errors on and off-glaciers, in the Lunana region, Bhutan Himalaya, during 2004–2011. The simulated surface mass balance (SMB) during 1979–2017, emergence velocity ( $v_e$ ) during 2002–2010, and rate of elevation change covering only the area of DGPS surveys are also indicated, along with observed number of  $1 \times 1$  m DEM cells ( $n$ ).

825

Glacier	$n$	Observed $dh$ (m)	Observed $dh/dt$ (m a <sup>-1</sup> )	SMB (m w.e. a <sup>-1</sup> )	$v_e$ (m w.e. a <sup>-1</sup> )	Simulated $dh/dt$ (m a <sup>-1</sup> )
Thorthormi	431	$-9.79 \pm 0.09$	$-1.40 \pm 0.01$	$-9.03 \pm 0.14$	$3.33 \pm 0.37$	$-5.81 \pm 0.87$
Lugge	248	$-32.70 \pm 0.12$	$-4.67 \pm 0.02$	$-6.77 \pm 0.17$	$-0.21 \pm 0.05$	$-7.62 \pm 0.72$
Off-glacier	3893	$0.48 \pm 0.03$				

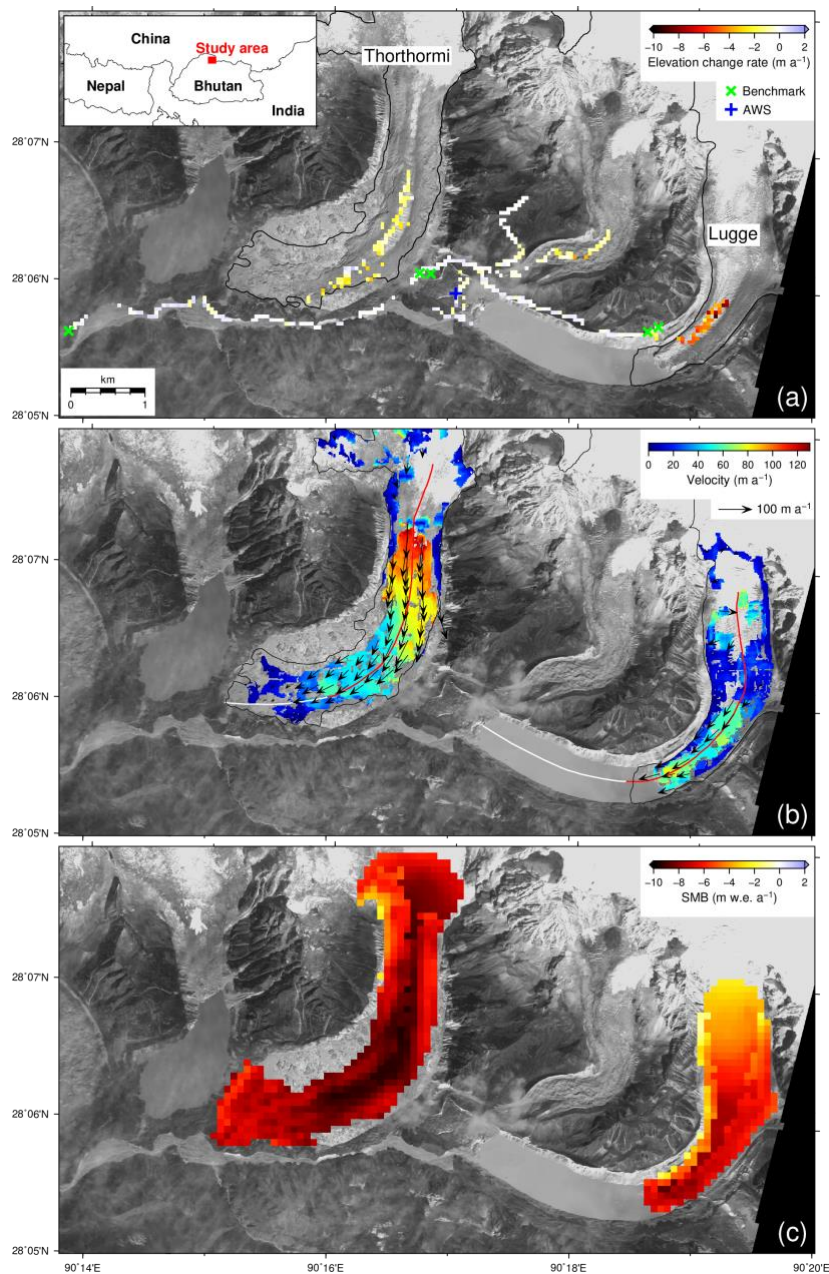


**Figure 1:** Glaciers and glacial lakes in the Lunana region, Bhutan Himalaya, superimposed with (a) the rate of elevation change for the 2004–2011 period, (b) surface flow velocities (arrows) with magnitude (colour scale), between 30 January 2007 and 1  
 830 January 2008, and (c) simulated surface mass balance (SMB) for the 1979–2017 period. The inset in (a) shows the location of the study site. The rate of elevation change in (a) is depicted on a 50 m grid, which is averaged from the differentiated 1 m DEMs. The light green crosses are the benchmark locations used for the GPS surveys in 2004 and 2011. The blue cross is the location of the automatic weather station installed in 2002 (Yamada et al., 2004). The black lines indicate the outline of the glaciers in November 2002. The background image is an ALOS PRISM scene from 2 December 2009. The white and red lines in (b) indicate the central flowline of each glacier, which is used for Figs. 3 and 6–8.  
 835

840

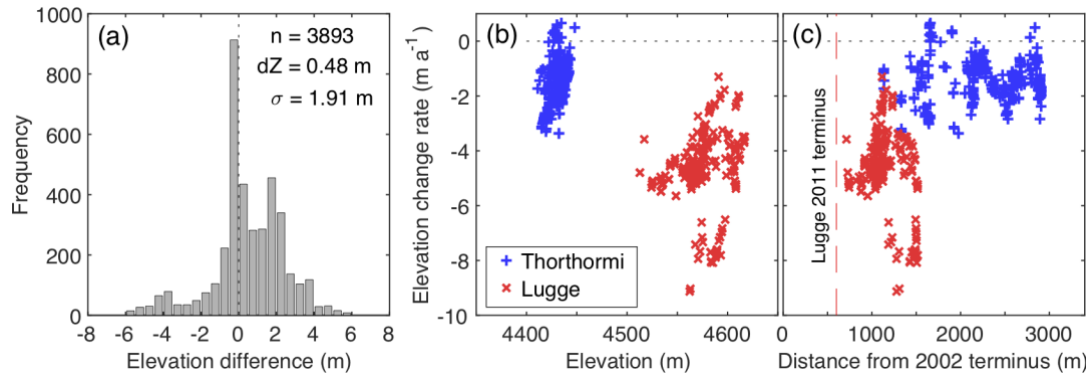
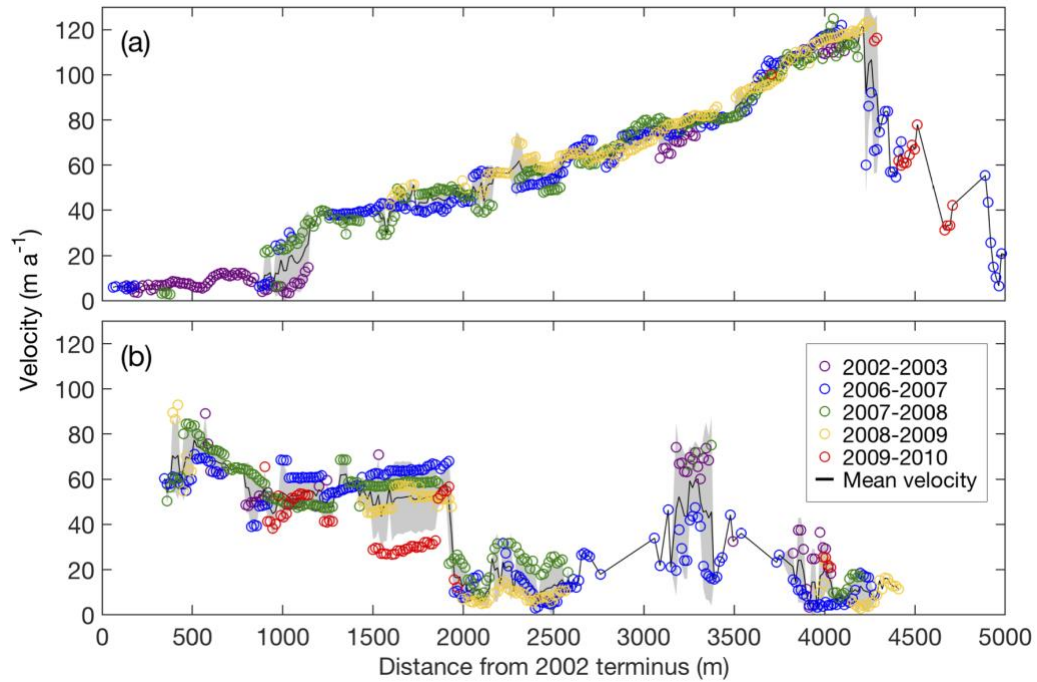


**Figure 2:** (a) Histogram of the elevation differences across off-glacier at 0.5 m elevation bins. The rate of elevation change  
845 for Thorthormi (blue) and Lugge (red) glaciers is compared with (b) elevation in 2011, and (c) distance from the glacier  
terminus in 2002 along the central flowlines (Fig. 1b). The red dashed line in (c) denotes the location of the calving front of  
Lugge Glacier in 2011.

850

855

860



870 **Figure 3:** Surface flow velocities along the central flowlines of (a) Thorthormi and (b) Luge glaciers for the 2002–2010 study  
 period. The black lines are the mean flow velocities from 2002 to 2010, with the shaded grey regions denoting the standard  
 deviation. The distance from each respective 2002 glacier terminus is indicated on the horizontal axis.

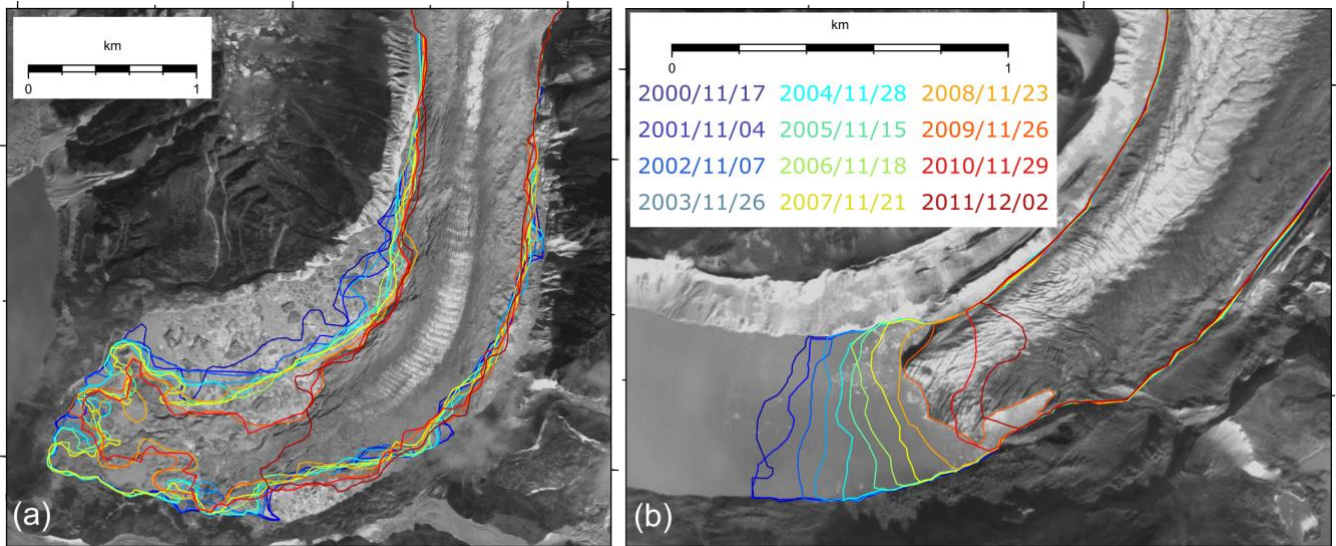
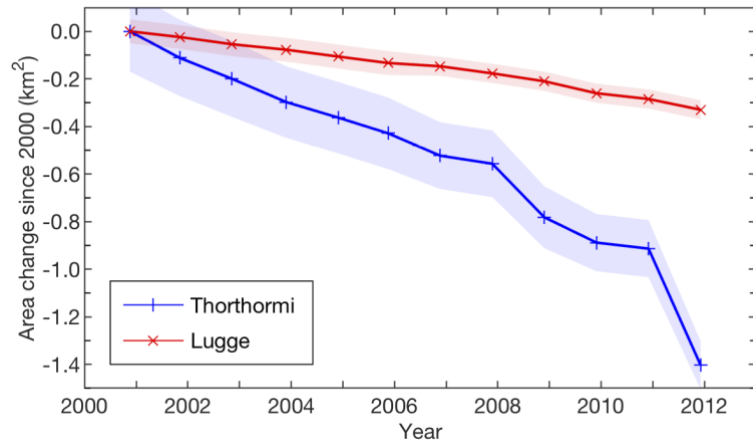


**Figure 4:** Glacier boundaries in the lower parts of (a) Thorthormi and (b) Luge glaciers from 2000 to 2011. The background image is an ALOS PRISM image acquired on 2 December 2009.

905



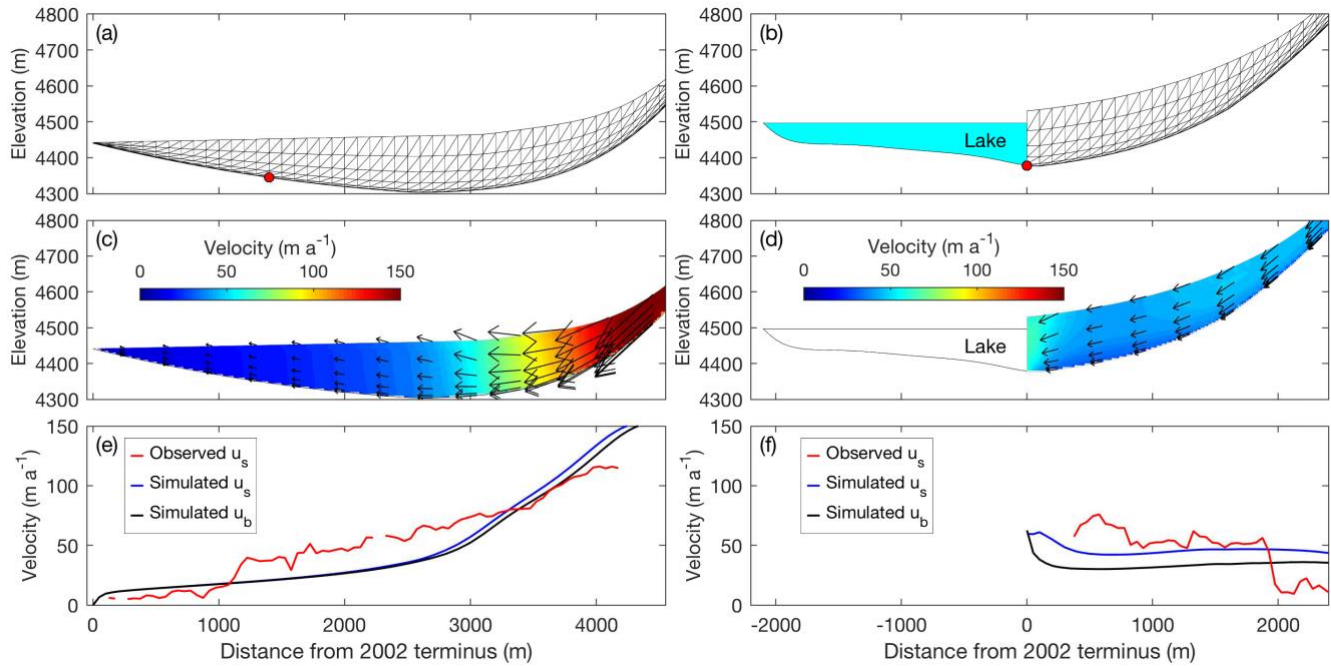
910

**Figure 5:** Cumulative area changes of Thorthormi (blue) and Lugge (red) glaciers since 17 November 2000. The shaded regions denote the uncertainties in the glacial area delineation.

915

920

925



935 **Figure 6:** Ice flow simulations in longitudinal cross sections of Thorthormi (left panels) and Luge (right panels) glaciers, with the present geometries of the glaciers employed in the models. (a and b) Finite element meshes used for the simulations, with red markers indicating the bedrock elevation based on a bathymetric survey. The light blue shading in (b) indicates Luge Glacial Lake. Simulated (c and d) two-dimensional flow vectors (magnitude and direction) and (e and f) horizontal components of the flow velocity. The blue and black curves are the simulated surface ( $u_s$ ) and basal velocities ( $u_b$ ), respectively. The red

940 curves are the observed surface flow velocities for 2002–2010.

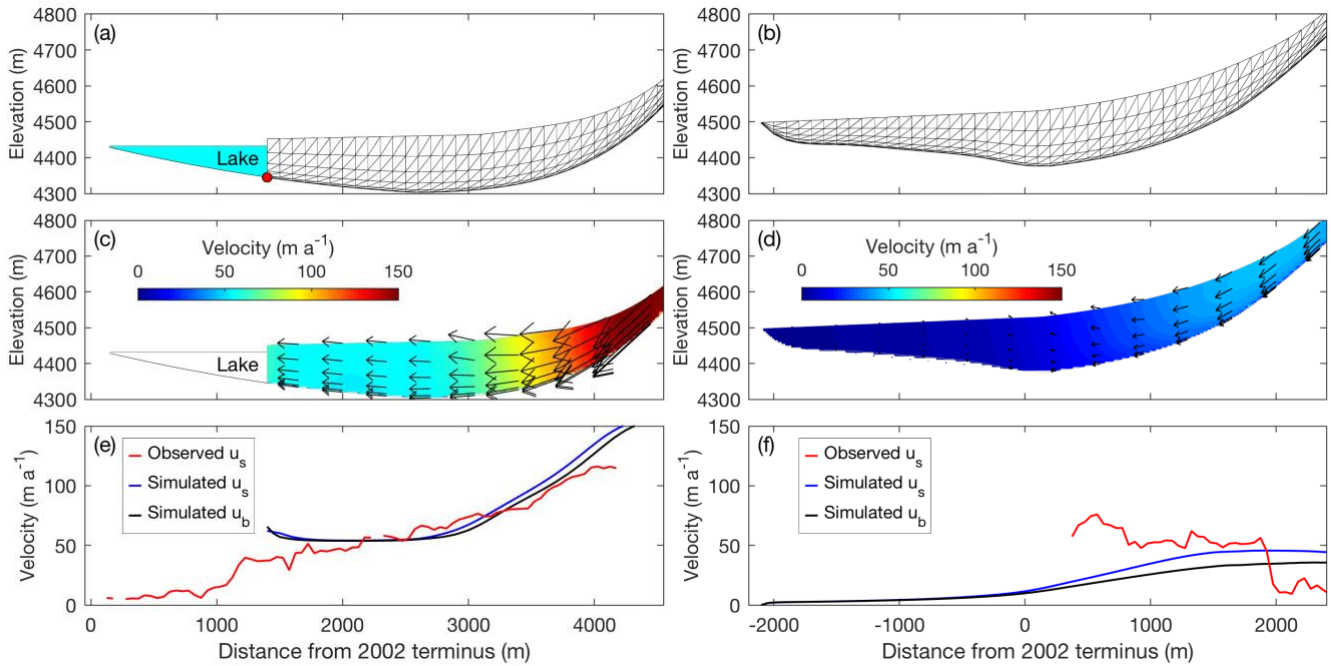


**Figure 7:** Ice flow simulations in longitudinal cross sections of Thorthormi Glacier under the lake-terminating condition (left panels), and Luge Glacier under the land-terminating condition (right panels). (a and b) Finite element meshes used for the simulation. The light blue shading in (a) indicates the proglacial lake in front of Thorthormi Glacier. Simulated (c and d) two-dimensional flow vectors (magnitude and direction) and (e and f) horizontal components of the flow velocity. The blue and black curves are the simulated surface ( $u_s$ ) and basal velocities ( $u_b$ ), respectively. The red curves are the observed surface flow velocities for 2002–2010.

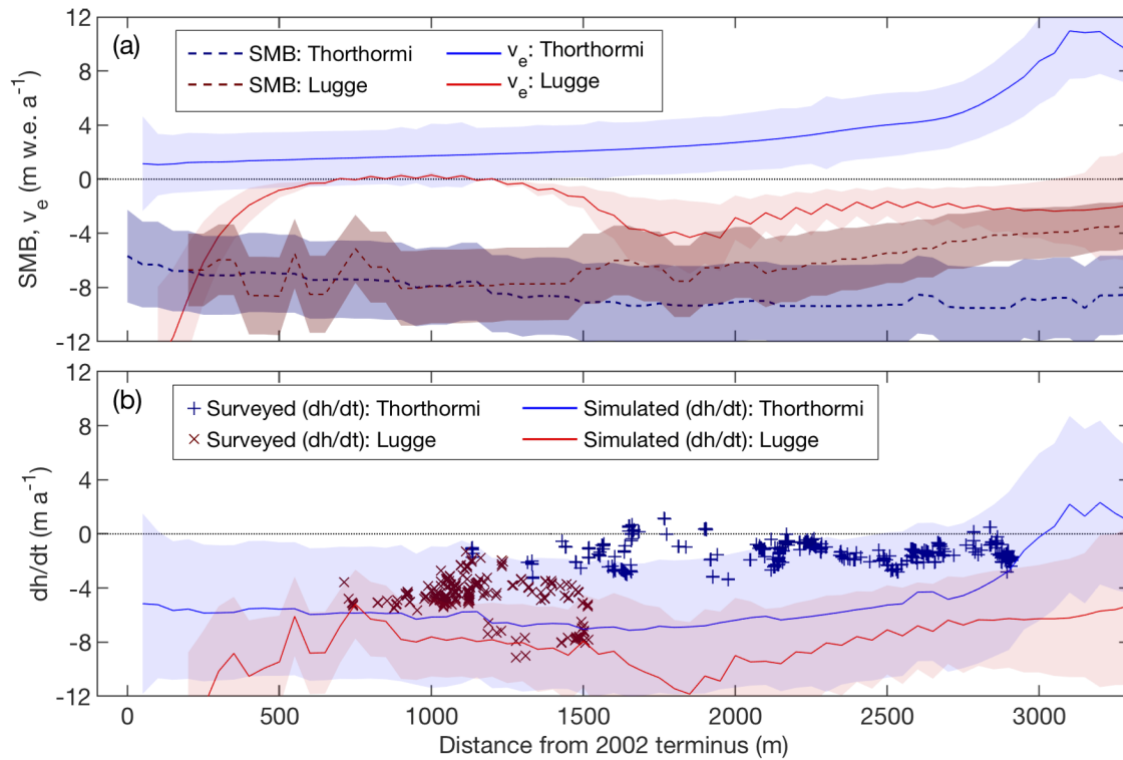


**Figure 8:** (a) Simulated surface mass balance (SMB) and emergence velocity ( $v_e$ ) calculations along the central flowlines of Thorthormi and Lugge glaciers. (b) Rate of elevation change ( $dh/dt$ ), as determined from DGPS surveys during 2004–2011 (marks) and model simulations (lines). Shaded regions denote the model uncertainties for each calculation.